Predicting landscape-scale CO_2 flux at a pasture and rice paddy with long-term hyperspectral canopy reflectance measurements

Jaclyn Hatala Matthes[1]*, Sara H. Knox[2], Cove Sturtevant[2], Oliver Sonnentag[3], Joseph Verfaillie[2], Dennis Baldocchi[2]

[1] Dept. Geography, Dartmouth College, 6017 Fairchild, Hanover, NH, USA

[2] Dept. Environmental Science, Policy, and Management, University of California – Berkeley, Berkeley, CA, USA

[3] Dépt. Géographie, Université de Montréal, Montréal, Canada

* Corresponding Author: jaclyn.h.matthes@dartmouth.edu

Abstract

Measurements of hyperspectral canopy reflectance provide a detailed snapshot of information regarding canopy biochemistry, structure and physiology. In this study, we collected five years of repeated canopy hyperspectral reflectance measurements for a total of over 100 site visits within the flux footprints of two eddy covariance towers at a pasture and rice paddy in Northern California. The vegetation at both sites exhibited dynamic phenology, with significant inter-annual variability in the timing of seasonal patterns that propagated into inter-annual variability in measured hyperspectral reflectance. We used partial least-squares regression (PLSR) modeling to leverage the information contained within the entire canopy reflectance spectra (400-900nm) in order to investigate questions regarding the connection between measured hyperspectral reflectance and landscape-scale fluxes of net ecosystem exchange (NEE) and gross primary productivity (GPP) across multiple timescales, from instantaneous flux to monthly-integrated flux. With the PLSR models developed from this large dataset we achieved a high level of predictability for both NEE and GPP flux in these two ecosystems, where the R^2 of prediction with an independent validation dataset ranged from 0.24 to 0.69. The PLSR models achieved the highest skill at predicting the integrated GPP flux for the week prior to the hyperspectral canopy reflectance collection, whereas the NEE flux often achieved the same high predictive power at the daily- through monthly-integrated flux timescales. The high level of predictability achieved by PLSR regression in this study demonstrated the potential for using repeated hyperspectral canopy reflectance measurements to help partition NEE measurements into its component fluxes, GPP and ecosystem respiration, and for using quasi-continuous hyperspectral reflectance measurements to model regional carbon flux in future analyses.

1. Introduction

The development of remote sensing tools that bridge the scale of carbon flux measurements from individual eddy covariance towers to broader, continuous spatial scales has long been a goal of the earth systems science community (Bauer, 1975; Running et al., 1999; Ustin et al., 2004). This goal inspired the formation of the international research group SpecNet, developed to synthesize the collection of near-surface ground reflectance measurements at eddy covariance tower sites to provide a crucial link between the spatial scales of eddy flux towers and aircraft or satellite measurements (Gamon et al., 2010). Previous work in near-surface remote sensing has demonstrated that normalized canopy reflectance indices can yield important insights for understanding landscape-scale CO_2 flux measurements, particularly for understanding patterns in CO_2 uptake through photosynthesis (Gamon et al., 1997; Inoue et al., 2008). Recent work has also demonstrated the utility of using the entire reflectance spectrum to uncover new normalized near-surface reflectance indices that are correlated with ecosystem productivity and can be used to monitor canopy phenology with relatively inexpensive LED sensors (Ryu et al., 2010a). Metrics based on canopy reflectance can be used as proxies for biological processes at the surface when those biological processes have corresponding features that change the reflectance and absorption of energy in the plant canopy. The two most commonly used remote sensing metrics, the normalized difference vegetation index (NDVI) and the enhanced vegetation index (EVI), track ecosystem productivity by measuring energy absorption at the visible wavelengths where chlorophyll is active and comparing that to the reflectance or emission at near-infrared wavelengths where active plant canopies dissipate energy (Liu and Huete, 1995; Rouse et al., 1974). NDVI and EVI are widely used metrics since they can be calculated worldwide (although at coarse spatial resolution of about 250m) by reflectance measurements from the Moderate-Resolution Imaging Spectroradiomenter (MODIS) instruments. The widespread use of normalized indices has revolutionized the predictive power of global carbon flux measurements, as they act as important proxies for photosynthetic carbon dioxide uptake in plants that can be modeled through temporally quasi-continuous satellite imagery (Justice et al., 1985; Potter et al., 1993; Running and Nemani, 1988; Tucker et al., 1985).

While these normalized indices have wide utility for predicting landscape-scale carbon flux at spatial scales from that of near-surface sensors to satellite remote sensing, these indices necessarily leave out much of the information provided within the entire visual and near-infrared spectrum of canopy reflectance. Modeling techniques such as partial least-squares regression (PLSR) (Wold et al., 2001) that can leverage the entire information contained within the quasi-continuous canopy reflectance spectrum by reducing the regression variables to a set of fewer latent variables (i.e. modeled variables that capture information from many individual regression variables at once) are now widely used to predict traits at the leaf, plot, and canopy level. Hyperspectral reflectance measurements have been used with PLSR methods to successfully predict leaf-level traits like nitrogen (N) and carbon content, specific leaf area, protein, cellulose, and lignin content, and even leaf isotopic ^{15}N content and Vcmax, the maximum rate of carboxylation during photosynthesis (Asner and Martin, 2008a; Bolster et al., 1996; Serbin et al., 2012, 2014). PLSR has also been used with near-surface canopy hyperspectral reflectance measurements to predict biomass and nitrogen content in wheat crops (Hansen and Schjoerring, 2003) and to predict pasture forage quality (Kawamura et al., 2008). Airborne hyperspectral reflectance measurements have been used with PLSR to map canopy-level chemistry (Ollinger et al., 2002; Smith et al., 2002), to predict citrus yields in orchards (Ye et al., 2009), and to map floristic gradients in grasslands (Schmidtlein et al., 2007) and species diversity in tropical forests

(Asner and Martin, 2008b). This large range of studies across a diverse set of spatial scales, from the leaf- to canopy-level, demonstrates the utility of using hyperspectral reflectance measurements in conjunction with PLSR methods to increase the predictive power of remote sensing relationships with ecological variables compared with traditional normalized indices. Despite the proven utility of PLSR methods over a wide range of spatial scales, to our knowledge no studies have yet investigated the potential for using hyperspectral reflectance measurements to directly predict landscape-scale carbon fluxes through PLSR modeling.

The goal of this analysis was to investigate the ability of repeat canopy hyperspectral reflectance to directly predict landscape-scale carbon dioxide (CO_2) fluxes at two short-structured plant canopies. We measured replicated near-surface hyperspectral canopy reflectance on 100 different sampling dates over the course of five years from 2010-2014 within the flux footprint of two nearby eddy covariance tower sites with similar structure but different canopy phenology in Northern California. The first site was a pasture where grasses grew over the winter and the invasive pepperweed plant (*Lepidium latifolium*) was active throughout the summer. The second site was an irrigated rice paddy with a simple phenology, where rice plants were present only from May through October following the typical growing season pattern for agricultural crops within this region. We combined the rich information contained within these repeated hyperspectral canopy reflectance measurements with PLSR methods to predict landscape-scale patterns in net CO_2 flux (net ecosystem exchange; NEE) and CO_2 uptake through canopy photosynthesis (gross primary productivity; GPP).

We used this five-year long-term dataset of near-surface hyperspectral canopy reflectance measurements collected at two sites in conjunction with landscape-scale eddy covariance CO_2 fluxes to answer the following four research questions:

1) How does canopy hyperspectral reflectance vary seasonally and inter-annually within and across sites during different phenological stages?

2) How well can the quasi-continuous 400-900nm canopy reflectance spectrum predict GPP and NEE at the two sites?

3) Are there significant differences in the ability to predict GPP and NEE at the pasture site compared with the rice paddy?

4) At what timescale are fluxes most strongly correlated with changes in measured hyperspectral canopy reflectance?

First, we examined the variability in measured hyperspectral reflectance within each site and between the two sites on individual sampling dates and across years. This provided insight into the dynamic nature of the canopy reflectance spectrum at these two study sites. The second two questions addressed the ability of the hyperspectral reflectance spectra to capture changes in GPP and NEE at the two sites, and tested whether the predictive power of hyperspectral reflectance modeling with PLSR is higher at the rice paddy site, where GPP and ER are more closely coupled than at the pasture, where GPP and ER are more decoupled due to different environmental drivers (Hatala et al., 2012; Knox et al., 2014). The final research question investigated the temporal scale at which the measured hyperspectral canopy reflectance integrated previous CO_2 fluxes. The canopy traits that control hyperspectral reflectance (e.g. chlorophyll, nitrogen, and water content in leaves, leaf abundance, etc.) are the emergent, integrated response to previous ecophysiological variability. We tested the ability of the canopy reflectance to predict instantaneous fluxes, and daily-, weekly-, and monthly-integrated carbon fluxes at each of the sites to quantify the timescale at which the canopy reflectance integrated prior ecophysiology, providing insight into the system memory of canopy reflectance. These three integrated flux timescales represented the peaks in temporal autocorrelation due to daily fluctuations in the diurnal cycle of plants and solar radiation, weekly fluctuations in synoptic weather fronts, and monthly variability due to seasonal and phenological patterns, respectively (Baldocchi et al., 2001b; Stoy et al., 2009). Together, these research questions yielded key insights into the utility and limitations of using repeated hyperspectral canopy reflectance measurements to predict landscape-scale CO_2 fluxes.

2. Methods

2.1 Site Characteristics

We collected replicated hyperspectral ground reflectance measurements of plant canopies at two sites in Northern California with similarly structured, yet phenologically different, plant canopies. The first site was a drained peatland pasture (hereafter referred to as "Pasture") located on Sherman Island in the Sacramento-San Joaquin Delta (latitude: 38.0373; longitude: -121.7536; elevation: -4m) with annual grasses growing during the winter and spring, and the invasive perennial pepperweed plant (*Lepidium latifolium*) active from spring through autumn (Figure 3). Pepperweed produces a dense canopy of white flowers each year from about the beginning of June through the end of August, creating increased complexity in canopy reflectance during this time (Sonnentag et al., 2011a, 2011b). The second site was a rice paddy (hereafter referred to as "Rice") located on Twitchell Island in the Sacramento-San Joaquin Delta (latitude: 38.1055, longitude: -121.6521, elevation: -5m) with an active growing season from May through October and maintained as a fallow and flooded field for the remainder of the year (Figure 3).

The two sites were located within 10km of each other in the Sacramento San-Joaquin Delta, and as such, they experienced the same Mediterranean climate with hot and dry summer months and rainy, cool winters. The 30-year mean annual air temperature (1981-2010) recorded at a nearby climate station in Antioch, CA was 16.4°C, and mean annual precipitation was 335mm. Despite their similar climatology, the difference in hydrological and agricultural management between the two sites results in ecosystems with plant canopies that are quite different in phenology (Hatala et al., 2012; Knox et al., 2014). The water table at the Pasture was maintained at a level always below the soil surface at around 50-80cm throughout the year. While the phenology of grasses at the Pasture peaked during the springtime, the pepperweed plants at the site remained relatively active throughout the summer as their roots can tap the shallow water table, creating a biologically active canopy almost year-round (Sonnentag et al., 2011a). The Rice was planted and flooded through irrigation management during the summer growing season only, and the plant canopy sustained high rates of productivity during the precipitation-free summer months. The field remained fallow and flooded during the remainder of the year. Differences in the canopy phenology at both sites propagated into differences in the peak periods of photosynthesis, where peak GPP at the Pasture occurs April-May and peak GPP at the rice occurs August-September (Hatala et al., 2012; Knox et al., 2014).

2.2 Hyperspectral canopy reflectance sampling

At both the Pasture and Rice, hyperspectral canopy reflectance was collected with a fiber optic spectrometer (USB 2000; Ocean Optics, Dunedin, FL) with a detector range from 200-1100nm at a height of 1m above the mean canopy surface. The fiber optic sensor was filtered through a cosine corrector (CC-3-UV-S Spectralon) to ensure that the bi-hemispherical reflectance from the ground surface was measured at an angle normal to the sensor surface

(Nicodemus et al., 1977; Schaepman-Strub et al., 2006). We measured bi-hemispherical reflectance to minimize the contribution of background soil surfaces to the spectral signal, and we ensured that our reflectance signal was not comprised by low Sun zenith angles by sampling near midday (Meroni et al., 2011). For this analysis we constrained our data to 400-900nm due to large levels of noise at the detection edges of this instrument. The spectrometer was mounted on a tripod approximately one meter above the canopy and was connected via USB cable to a laptop computer running the OOBase32 software (USB 2000; Ocean Optics, Dunedin, FL) to capture spectra, which internally corrected for instrument-specific calibration parameters. Each field spectrum was collected and saved by OOBase32. At the start of each site visit, the integration time within OOBase32 was adjusted to the ambient light conditions and a reference dark spectrum measurement was collected by covering the fiber optic head with two layers of black electrical tape and orienting the sensor downward.

After this initial set-up, we collected a reflectance spectrum for each site replicate by first pointing the spectrometer directly skyward to record the spectrum of incoming energy, and within seconds, pointing the spectrometer directly at the ground surface to record the spectrum of reflected energy. Thus, we calculated the canopy reflectance for each replicate as the reflected spectrum normalized by the incoming spectrum. For each collection date at each site, we averaged the replicate spectra for this analysis to compute a single mean spectral reflectance per date at each site. The spectrometer records data at approximately 0.28nm intervals, and we smoothed each reflectance spectrum using a spline fit to 1nm intervals between 400-900nm in order to reduce instrumental noise in the data.

We measured canopy hyperspectral reflectance from July 2010 through September 2014 at both sites, collecting measurements during the entire year at the Pasture and during the growing season at the Rice, which amounted to 100 total sampling dates at the Pasture and 71 total sampling dates at the Rice (Figure 1). On each sampling date, hyperspectral reflectance measurements were collected at each site with a spatial and temporal replicate frequency suited to the individual site heterogeneity. At the Pasture, where the canopy was spatially and temporally heterogeneous, we measured hyperspectral reflectance approximately weekly, bi-weekly, or monthly, with nine replicate canopy reflectances randomly sampled per visit. At the Rice, which had lower spatial variability, hyperspectral reflectance was collected weekly or bi-weekly during the growing season, with five replicate canopy reflectance spectra collected per visit. We occasionally collected up to ten additional replicates at each of the sites, in order to ensure that our smaller sampling sizes were capturing broad landscape-scale patterns in spatial heterogeneity. At each site we randomly sampled canopy reflectance at locations approximately 10-20m within the flux tower footprint, the area most representative of the half-hourly flux measurements. For partial least-squared regression analysis, we averaged across the hyperspectral canopy reflectance replicates for each site and day. Because leaf geometry and clumping can critically impact the interpretation of canopy reflectance measurements (Colwell, 1974), these two sites provide a useful first-case study for directly connecting hyperspectral canopy reflectance measurements to CO_2 flux because both ecosystems have an erectophile in leaf angle distribution for the majority of the year, minimizing shadow effects when field spectra are collected near solar noon.

2.3 CO_2 flux measurements

Both sites are active AmeriFlux and FLUXNET sites (Baldocchi et al., 2001a) measuring fluxes of energy, water vapor, and CO_2 using standard eddy covariance methods and processing procedures described elsewhere in detail (Ameriflux site codes: US-Snd and US-Twt; Hatala et al., 2012; Knox et al., 2014; Sonnentag et al., 2011a). The eddy covariance technique was used to measure the fluxes of CO_2 at each site by collecting simultaneous 10 Hz measurements of vertical turbulence (*w*, m s^{-1}), measured with a sonic anemometer (Gill WindMaster Pro; Gill Instruments Ltd, Lymington, Hampshire, England), and CO_2 density (*c*, μmol m^{-3}), measured with an infrared gas analyzer (LI-7500; Li-Cor Biosciences, Lincoln, NE). From these measurements we calculated the net half-hourly mean flux of CO_2 (NEE, μmol m^{-2} s^{-1}) between the surface and atmosphere by averaging the covariance between *w* and *c* over a half-hourly time period after applying a coordinate rotation and a set of standard air density and temperature corrections (Detto et al., 2010; Schotanus et al., 1983; Webb et al., 1980). To partition NEE into gross primary photosynthesis (GPP, μmol m^{-2} s^{-1}) and ecosystem respiration (ER, μmol m^{-2} s^{-1}), net CO_2 fluxes were first gap-filled using artificial neural network (ANN) techniques outlined in detail within Knox *et al.* [2014], driven by meteorological variables (Moffat et al., 2007; Papale et al., 2006). After the net CO_2 fluxes were gap-filled using the ANN technique, we separated the net flux into GPP and ER by modeling nighttime NEE measurements as ER, since GPP is assumed to be zero at night (Reichstein et al., 2005). We prescribed the nighttime temperature dependence of ER by an Arrhenius-type model (Lloyd and Taylor, 1994), and extrapolated this model to the daytime, calculating GPP as the difference between NEE and modeled ER. Net CO_2 flux data within this analysis are presented from the atmospheric convention, where a negative flux indicates ecosystem uptake, and a positive flux indicates release from the ecosystem to the atmosphere.

Within this analysis we examined the predictive power of hyperspectral canopy reflectance to explain patterns in instantaneous and daily-, weekly-, and monthly-integrated NEE and GPP flux. We tested these variables separately in order to determine whether the canopy reflectance better predicted an instantaneous flux measurement at the time of collection, or a flux signal integrated over the previous day, week, or month. For instantaneous NEE and GPP flux, we matched the time of spectral collection with the nearest mean half-hourly flux measurement, where these values are presented in units of μmol m^{-2} s^{-1}. For the daily-, weekly-, and monthly-integrated NEE and GPP fluxes, we integrated the net CO_2 and GPP flux over the course of the previous day, week, or month for the date of spectral reflectance collection, where these values are presented in units of g-C m^{-2} $time^{-1}$. For reference regarding the magnitude and temporal dynamics of CO_2 fluxes at the Pasture and Rice, the instantaneous GPP flux and daily NEE flux for both sites are plotted as Figure 2.

2.4 Partial Least-Squares Regression Modeling

Partial least-squares regression is a standard method in chemometrics for modeling the ability of a set of quasi-continuous spectral variables to predict a single response (Wold et al., 2001). In this analysis we used PLSR methods with the hyperspectral canopy reflectance dataset to model the response of instantaneous or integrated NEE or GPP. PLSR is similar to principle components analysis (PCA), in that the modeling algorithm reduces a large predictor matrix of spectral reflectance data to a reduced set of latent variables. In our study, the large predictor matrix is the measured hyperspectral reflectance at each wavelength between 400-900 nm during each sampling event, which in our analysis was reduced to a maximum of 10 latent variables that contained the most significant sets of variables from the larger matrix for predicting instantaneous or integrated NEE or GPP. PLSR typically outperforms PCA or standard step-wise linear regression for situations where there is high co-linearity within the predictor matrix, such as within narrow-band spectral reflectance and chemometrics (Wold et al., 2001). For this analysis we used the PLS package (Mevik et al., 2013) within the R statistical environment (R

Development Core Team 2014). All the R code used to conduct this analysis is freely available on GitHub at http://github.com/jhmatthes/canreflectance_flux_plsr.

For PLSR model fitting and validation, our methods followed those of Serbin *et al.* (2014), which used PLSR regression modeling to determine the ability of hyperspectral reflectance data to predict a suite of leaf traits. However, in this analysis, we used repeated measurements to examine how well the repeated hyperspectral reflectance measurements could directly predict landscape-scale fluxes of NEE and GPP. We conducted one set of PLSR regression modeling for the entire spectral reflectance dataset that combined both the Pasture and Rice data, and then two additional PLSR modeling exercises with the only the Pasture data and only the Rice data, to examine whether there were significant differences between the two sites in the resulting PLSR models. For each of the three PLSR modeling exercises, we split the data into model calibration (80% of the data) and independent validation (20% of the data; hereafter referred to as “Independent Validation”), where the model calibration data were used to fit the model, and the independent validation data were used to evaluate the ability of the model to predict landscape-scale NEE and GPP outside of the PLSR model fitting exercise. As in Serbin *et al.* [2014], we randomly split the model calibration data into 70% for model fitting (hereafter referred to as “Calibration”) and 30% for model uncertainty evaluation (hereafter referred to as “Evaluation”) over 1000 iterations to evaluate the uncertainty in PLSR model development. So overall, we used 56% of the total data for Calibration, 24% of the data for Evaluation, and an unchanging 20% of the data for Independent Validation to test the predictive power of the final mean models. We conducted an initial optimization with a single set of Calibration data and Evaluation data to determine the total number of PLSR latent variables to include in each model by minimizing the prediction residual sum of squares, calculated through leave-one-out crossvalidation (Chen et al., 2004). We used the entire 400-900nm spectrum range with these PLSR methods to fit the instantaneous and daily-, weekly-, and monthly-integrated NEE and GPP flux data.

To quantify the performance of each PLSR model we calculated the coefficient of determination (R^2), the root mean square error (RMSE), and the model bias. We used the 1000 iteration bootstrapping approach for each PLSR to quantify the model calibration performance as in Serbin *et al.* [2014]. From the random 70% to 30% split of the Calibration and Evaluation data, we generated new estimates for each iteratively removed sample. This allowed us to test the stability and generality of the models using different sets calibration data and to estimate robust errors for the prediction of flux measurements by representing the uncertainty across measurements, spectral data, and the PLSR modeling approach. For each set of 1000 modeling iterations over the random calibration/validation fit dataset split, we calculated the resulting mean PLSR model coefficients and the variable importance of projection (VIP) score associated with the reflectance measured at each wavelength. The VIP score represents the statistical contribution of each individual wavelength to the overall fitted PLSR model across all latent model components. In this way, the VIP score can be used to identify the wavelengths that contribute the most information for predicting the variable at hand (in this case, either NEE or GPP). Using the mean of the bootstrapped PLSR models, we tested each final mean model against the 20% of original data left aside for Independent Validation by linear regression.

2.5 Standardized vegetation indices for GPP and NEE prediction

We analyzed the skill of standardized vegetation indices (SVIs) in predicting NEE and GPP flux at the Pasture and Rice, and compared the utility of these models to our PLSR modeling results. Due to their wide use in other studies, we tested the normalized difference vegetation index (NDVI; $[R_{800} - R_{680}]/[R_{800} + R_{680}]$; Rouse et al., 1974), NDVI calculated with the wavelengths from the Moderate Resolution Imaging Spectroradiometer satellite ($NDVI_{MOD}$; $[R_{841\text{-}876} - R_{620\text{-}670}]/[R_{841\text{-}876} + R_{620\text{-}670}]$), green NDVI ($NDVI_g$; $[R_{800} - R_{550}]/[R_{800} + R_{550}]$; Gitelson et al., 1996), red-edge NDVI ($NDVI_{re}$; $[R_{800} - R_{700}]/[R_{800} + R_{700}]$; Gitelson and Merzlyak, 1994), and the photochemical reflectance index (PRI; $[R_{531} - R_{570}]/[R_{531} + R_{570}]$; Gamon et al., 1992), where R indicates reflectance in the subscripted wavelengths in nanometers. For all SVIs except $NDVI_{MOD}$, we averaged the measured reflectance for a 10nm window centered on the reflectance value to reduce measurement noise.

We assessed the ability of SVI measurements to predict NEE and GPP fluxes for All data, the Rice only, and the Pasture only by randomly selecting 80% of the reflectance spectra for calibration, leaving 20% of the data for prediction. For GPP fluxes, we assessed the fit and prediction of SVIs with a log-linear model as this model best fit the data, and for NEE we used a simple linear model, which fit the data better than a log-linear model. To assess the ability of the SVIs to predict GPP and NEE, we performed an iterative calibration/prediction analysis where we randomly parsed the data into 80% calibration and 20% prediction for 100 iterations, and present the mean statistics for comparative analysis with the PLSR modeling results.

3. Results

3.1 Spatiotemporal variability in hyperspectral canopy reflectance

There was significant seasonal, inter-annual, and site-level variability across the hyperspectral canopy reflectance measurements collected over the course of five years at both sites. Intra-site variability within canopy reflectance changed due to the phenological stage of the ecosystem, whereas inter-annual variability was driven by changes in the timing of these phenological events. The Pasture tended to be more spatially heterogeneous than the Rice, observed through the higher intra-site variability during an individual sampling event, particularly in the infrared reflectance (Figure 3). This intra-site variability at the Pasture is caused by higher spatial heterogeneity in canopy structure compared with the Rice, which is a monoculture with a simpler crop phenological cycle. During the green leaf-out stage at both the Pasture and Rice, the patterns of hyperspectral reflectance were quite similar, with a peak at the green wavelengths, absorption in the red wavelengths, and high reflectance in the near-infrared wavelengths (Figure 3a,b). Intra-site variability across the spectrum was high across at the Pasture during periods of white pepperweed flowering that produced a much higher albedo than the green canopy and obscured reflectance patterns in the green and red wavelengths, despite relatively high plant productivity during this time (Figure 3c). The closest analogous phenological stage to this period at the Rice was during the time at which the rice has seeded and the plants have dried in preparation for harvest, when the Rice experienced similar trends in increased albedo through the visible wavelengths (Figure 3d). However, the magnitude of the senescing Rice reflectance was not as large as the white pepperweed canopy at the Pasture, and in addition the reflectance spectra were not obfuscated during this time since the rice productivity was quite low at this point in the growing season.

The seasonal and inter-annual patterns in narrow-band reflectance in the green (550±5 nm), red (640±5 nm), and near-infrared (NIR; 800±5 nm) wavelengths also highlighted intra-site and inter-annual variability. At the Pasture, there was low intra-site variability and inter-annual variability in green reflectance from January through the end of May, when the grass canopy was present at the site (Figure 4a). However, when pepperweed became the dominant canopy plant at the Pasture during the summer growing season, both replicate and inter-annual variability increased as the pepperweed created a more heterogeneous cover than the grass due to its white flowers and more spatially variable structure than the winter grass canopy. The same pattern was evident in the red reflectance at the Pasture, with low variability in the second half of winter and spring, and a large increase in variability during the summer growing season and autumn (Figure 4c). At the Rice, there was also large inter-annual variability in the timing of the seasonal pattern green and red reflectance, however there was a more discernible seasonal pattern of reflectance that tracks within years across the entire growing season (Figures 4b,d). For example, each year green reflectance and red reflectance started high, decreased as the growing season progressed, then eventually increased again as the rice straw dried before harvest. The NIR reflectance at the Pasture had a stable mean through the year with little inter-annual variability but large intra-site variability across the year (Figure 4e). The Rice NIR reflectance had a consistent seasonal pattern between years, with low reflectance in the early growing season and increasing NIR reflectance as the canopy developed due to the change in the rice canopy closure as the growing season progressed (Figure 4f). Although there was a consistent phenological trend in NIR reflectance at the Rice each year, there remained inter-annual variability in the timing of the NIR minimum and larger intra-site variability compared with reflectance in the visible wavelengths.

3.2 Calibrated PLSR models for predicting NEE and GPP

We fit PLSR models to the hyperspectral data to predict landscape-scale NEE and GPP at four integrated flux timescales: instantaneous flux measurements, and daily-, weekly-, and monthly-integrated flux measurements for the period preceding the time of hyperspectral canopy reflectance collection. In this analysis we determined the optimal number of latent variables to include for each model by minimizing the predictive residual sum of squares. The number of optimal latent variables included in the PLSR models ranged from 2-8, which indicated that some models could achieve the best predictive statistical fit for NEE and GPP with a much lower number of components than other models (Table 1). For the PLSR models that included the entire canopy reflectance dataset for both sites, the optimal number of latent variables was stable at six components, except for the instantaneous GPP model, which included seven components. The number of optimal components was more variable across the PLSR models for the Pasture reflectance data (2-8 components) compared with those from the Rice reflectance data (4-6 components).

As expected, across all models, the R^2 for the PLSR Calibration was higher than the R^2 for the PLSR Evaluation fit, and the RMSE was lower for the Calibration and higher for the Evaluation during the model calibration step (Table 1). The fit statistics presented within Table 1 show the mean fit statistics for the 1000 iterations of random 70% Calibration, 30% Validation data selection from the 80% total data used during the model development fitting process. For each PLSR model, the 1000 iterated fit statistics followed a normal distribution with low variance, which indicated only a low bias to selecting the Calibration and Evaluation data so only the mean results are presented within Table 1. Across almost all of the CO_2 flux prediction variables, the PLSR models for the Rice dataset achieved the highest fit for both the Calibration (R^2 = 0.77-0.92) and Evaluation (R^2 = 0.58-0.68) exercises, the PLSR models with the dataset including both sites achieved a slightly lower overall fit for Calibration (R^2 = 0.63-0.87) and Evaluation (R^2 = 0.24-0.69), and the PLSR models for the Pasture had the lowest overall fit for Calibration (R^2 = 0.38-0.97) and Evaluation (R^2 = 0.29-0.56) (Table 1).

For each set of 1000 modeling iterations over the random calibration/validation fit dataset split, we calculated the resulting mean PLSR model coefficients and the variable importance of projection (VIP) statistic associated with each wavelength. Across all fitted PLSR models, as the timescale of the fitted integrated flux increased from instantaneous to daily-, weekly-, and monthly-integrated values, the VIP statistic in the visible wavelengths (400-700nm) decreased and the VIP statistic in the near-infrared wavelengths (700-900nm) increased (Figure 5). This indicated that for flux measurements on short timescales, the reflectance in the visible wavelengths contributed the highest explanatory power to the PLSR model components, but at longer timescales structural changes in the canopy that are correlated with the NIR range became more important for predicting GPP and NEE flux. This pattern was especially apparent for the VIP scores of the GPP model using the dataset with both sites (Figure 5a), where there was a dramatic shift in VIP scores between the weekly- and monthly-integrated flux models. For the weekly-integrated GPP flux model and those at shorter timescales, the highest VIP scores were contributed by the visible wavelengths, with a peak in the red wavelengths near 700nm. However for the monthly-integrated GPP flux model, there was a dramatic difference where the highest VIP scores shifted from the visible to the NIR range, indicating that structural components of the plant canopy correlated with NIR reflectance contributed higher predictive power than reflectance in the visible part of the spectrum. There is a lower shift in VIP scores across integrated flux timescales in the models developed with only the Rice dataset (Figure 5e-f) compared against the models developed with only the Pasture dataset (Figures 5c-d), likely reflecting the increased spatial and phenological complexity of the Pasture ecosystem compared with the relatively homogeneous Rice.

Across all models, the visible wavelengths that contributed the most information to the PLSR models, as determined by the magnitude of the VIP score, were within the red portion of the visible spectrum (Figure 5). Most PLSR models had VIP scores above 1.0 that correlated with reflectance at 642 and 662 nm, the wavelengths of chlorophyll absorption. Across most

PLSR models there was also a peak in the VIP score near 673 nm, the wavelength of chlorophyll fluorescence. However, the second band of chlorophyll fluorescence at 726nm, exhibited low VIP scores across all models. For both of the PLSR models developed using only the Pasture dataset, there were also high VIP scores within the violet and blue range of the visible spectrum, from 400-450nm. These high VIP scores in the violet-blue portion of the spectrum could be partly explained by the chlorophyll a and b absorption peaks at 430nm and 460nm, because slightly higher VIP scores were also observed at the Rice site for these wavelengths (Figure 5e-f). However, this part of the spectrum at the Pasture site was particularly significant compared with the other models, and this could correspond to white reflectance of the pepperweed flowers at the site. When the pepperweed canopy was blooming, the bright white flowers reflected light across the entire visible spectrum, a unique characteristic to this site, where the high visible albedo in this spectral range might also have contributed to the high VIP scores within this portion of the spectrum (Figure 5c-d).

3.3 Independent Validation of PLSR models for NEE and GPP

After we fit the PLSR models to 80% of the entire dataset through 1000 iterations of different random sets of Calibration and Evaluation data, we tested the mean fitted models against the Independent Validation data (the 20% of the original dataset left out of the PLSR model fitting process). In general, the fitted PLSR models achieved a good fit with the measurements for this Independent Validation dataset, where the R^2 fit between the predicted and actual NEE and GPP ranged from 0.26 to 0.69 (Table 2). As was the case for the calibration and validation R^2 fits during the PLSR calibration process, the Rice dataset achieved the highest R^2 values (0.40-0.69), the dataset with both sites achieved the second-highest set of R^2 (0.27-0.62), and the Pasture dataset had the lowest R^2 (0.27-0.54). As in the previous discussion for the

Calibration and Evaluation fits to these three sets of data, we believe that the lower level of predictability at the Pasture is due to the higher level of spatial heterogeneity and phenological complexity compared with the Rice.

Although all models achieved a statistically significant fit between the predicted and measured CO_2 fluxes with the Independent Validation dataset with relatively high R^2 values, the uncertainty in the prediction was significantly lower for the models that included all the data compared with the models that included only either the Pasture or Rice data. This pattern is clearly observed within the Independent Validation fit for the daily GPP and NEE data (Figure 6). For the daily prediction of both GPP and NEE, the dataset that included all the data had a smaller range for both the 95% confidence interval and 95% prediction interval for the relationship between predicted and actual GPP and NEE. This trend likely represented an increase in predictive power achieved by including a larger dataset with a wider range of values both for NEE and GPP and for the measured hyperspectral reflectance. As the datasets that included either the Pasture and Rice data only had a lower amount of data overall as well as a narrower range of values, the confidence in the ability to predict NEE and GPP at these individual sites was lower compared with the power of using the entire combined dataset.

3.4 Prediction of NEE and GPP fluxes with standardized vegetation indices

We compared the ability of a suite of commonly used SVIs to predict GPP and NEE with the skill of the mean PLSR models developed within this study. Overall, the suite of NDVI SVIs performed reasonably well at predicting both GPP and NEE, and models tested with all the reflectance data for both sites achieved predictive R^2 values that ranged from 0.18 to 0.59 (Table 3; Supplementary Table 1), where red-edge NDVI was the SVI that achieved the highest skill for predicting GPP and NEE for the sites in this study. PRI was not well suited to predicting CO_2

fluxes at these sites, and models for this SVI achieved predictive R^2 fits that ranged from 0.02 to 0.22.

For models that fit all the data from both sites, the predictive fit from PLSR modeling outperformed the red-edge NDVI (the best-fit SVI) at the instantaneous and weekly timescales, the two models were not significantly different at the daily timescale, and red-edge NDVI outperformed PLSR modeling at the monthly timescale (Table 3). PLSR modeling outperformed SVIs across all timescales for models that fit the Pasture data only. The performance of red-edge NDVI and PLSR models were not significantly different at instantaneous, daily, and weekly timescales when fit with the Rice data only, however red-edge NDVI was a better predictor of monthly CO_2 fluxes than the PLSR models (Table 3).

3.5 Prediction of NEE and GPP fluxes across different timescales

We investigated the ability of PLSR modeling with the hyperspectral canopy reflectance measurements to predict instantaneous GPP and NEE fluxes from the same half hour of spectral measurement, in addition to fluxes integrated over the previous day, week, and month. Previous work determined that sampling errors in eddy covariance flux measurements diminished when the fluxes were integrated over the course of many days (Moncrieff et al., 1996). We expected that the instantaneous flux would achieve the lowest correlation with the measured canopy reflectance since reflectance changes more slowly compared with CO_2 flux, and that the fluxes integrated over longer timescales would provide a stronger signal with a higher predictive capacity. For the Calibration and Evaluation during the initial PLSR model fitting, there was no strong evidence that one timescale (instantaneous, daily, weekly, or monthly flux) was particularly better fit with the hyperspectral canopy reflectance than the other timescales (Table 1). However, during the evaluation of the predictive power of the PLSR models with the

Independent Validation data, most models achieved the highest predictive R^2 with GPP flux at the weekly-integrated timescale, and we found no clear optimal timescale for predicting NEE with measured hyperspectral reflectance data (Table 2; Figure 7).

4. Discussion

4.1 Sources of variability in measured reflectance

Variation across the measured hyperspectral canopy reflectance was dominated by inter-annual variability in the timing of canopy phenology (Figures 3,4). At the Rice, transitions were typical for an agricultural crop, where canopy reflectance incorporated portions of the background flooded soil in conjunction with the emerging green plants early the in growing season, with canopy closure achieved by early July (Beget and Di Bella, 2007). After flooding when the Rice canopy closed, there was less intra-site variability in measured reflectance, until the end of the growing season when the rice plants started to senesce and dry before harvest (Figure 4). At the Pasture, canopy phenology was more complicated, marked by a transition from a green grass canopy to a green pepperweed canopy in April, followed by the white flowering of the pepperweed canopy from June through August, which increased intra-site variability in measured reflectance (Figure 4). Both the Rice and Pasture experienced significant inter-annual variability in the start and end dates of these phenological patterns, but despite this variability the sites experienced relatively low variability in the overall CO_2 flux (Figure 2). The primary driver of inter-annual variability at the Pasture was the timing of summer drought in the Mediterranean climate, and canopy management (Sonnentag et al., 2011a). These primary controls agreed with the results from European syntheses of FLUXNET sites where water was a key driver of inter-annual variability in NEE (Reichstein et al., 2007). At the Rice, inter-annual variability was driven by changes in the start and end dates of canopy phenology that were driven by changes agricultural management of the planting and harvesting dates each year and smaller changes in fertilizer management (Hatala et al., 2012; Knox et al., 2014). The timing of the planting and harvest at the Rice is controlled by logistical environmental drivers, as the field must be dry enough to drive farm equipment through the soil, and warm enough to ensure seedling survival. Differences in these variables from year to year created variability in the planting dates, and subsequent variability in the seasonal trajectory of hyperspectral canopy reflectance (Figures 3,4). There are also important differences between PLSR methods using the complete spectrum and standardized vegetation indices (SVIs) that may lead to differences in interpreting which bands are best suited for correlation with CO_2 fluxes. Because SVIs are normalized by a reference band, they may be better suited to reducing noise within temporal trends in reflectance time series, particularly at sites that experience a wide range of illumination conditions. While the PLSR methods used in this analysis benefit from the large information content that results from using the entire reflectance spectrum, the measurements represent relative reflectance values rather than normalized reflectance ratios, and thus likely include more noise in the measurement time series than SVIs. This is an important trade-off when considering whether to use the entire reflectance spectrum or SVIs to understand how canopy reflectance tracks CO_2 fluxes, but the simple canopy structure at the sites in this analysis and the collection of measurements during ideal illumination conditions limits the overall noise within the reflectance time series.

4.2 Predicting NEE & GPP with PLSR models

Along with the inter-annual variability experienced at both sites, there were also differences in the intra-site variability of measured reflectance within the two flux tower footprints. The Pasture site was more spatially heterogeneous than the Rice, driving increased variability among replicate hyperspectral reflectance spectra at the site (Figure 4). The increased spatial variability at the Pasture was reflected in the lower predictive power of the PLSR models in predicting GPP and NEE with only the Pasture dataset (Tables 1,2). The lower overall fit between the hyperspectral measurements and CO_2 flux at the Pasture can be explained through three possible mechanisms: 1) the hyperspectral canopy reflectance measurements at the Pasture are less representative of the entire flux footprint than the Rice data, 2) white pepperweed flowers in the Pasture canopy during summertime create an obstruction for reflectance that degrades the representativeness of measured spectra (Hestir et al., 2008; Sonnentag et al., 2011b), 3) the lack of irrigation at the Pasture compared with the Rice could create conditions of water stress during which reflectance becomes temporally decoupled from CO_2 flux. It is likely that all of these factors contributed to the lower PLSR predictive power at the Pasture, and in particular the obstruction by white canopy flowers presented a challenge that is somewhat unavoidable for canopy reflectance studies in complex ecosystems. Changes to future sampling efforts that address the footprint representativeness, for example increasing the number and spatial distribution of hyperspectral reflectance collected at the Pasture or flying an unmanned aerial vehicle (UAV) with a mounted hyperspectral sensor, might help to further improve the future PLSR predictive power.

The most important wavelengths for the PLSR modeling with the GPP and NEE flux data in this study fell in line with previous work that has examined correlations between reflectance and traits of photosynthetic uptake (Main et al., 2011). However, we were initially surprised to find that the green wavelengths were not dominant components for prediction of either NEE or GPP across the suite of calibrated PLSR models (Figure 5). These results do parallel recent work in oak forests that demonstrated a temporal mismatch between peak greenness and peak leaf chlorophyll content (Yang et al., 2014). This temporal mismatch could be the cause for the insignificant correlation in narrow-band green reflectance, because at both sites vegetation is a lighter green early in the growing season and develops into a darker green as the season progresses. There were particularly high VIP scores in the blue visible wavelength range, from 400-450 nm, at the Pasture site (Figure 5c,d), which could be partly explained by the chlorophyll a and b absorption peaks at 430nm and 460nm since the Rice also experienced slightly higher VIP scores in this region (Figure 5e-f). However, the magnitude of the VIP scores in this region at the Pasture far exceeded those at the Rice. There are two possible explanations for this marked increase in the importance of the blue visible wavelengths at the Pasture: 1) white reflectance of the pepperweed flowers at the site could be increasing the albedo within this portion of the spectrum; 2) the more complex phenology at the site with annual grass and pepperweed senescence is periodically driving reflectance near 420 nm in response to these periods of stress (Carter and Miller, 1994). While the Pasture shifted toward much higher reflectivity across the visible wavelengths during the brief period of white flowering in late spring (Figure 3a), this site also experienced more dynamic phenology overall, with browning of the grass in early summer and of the pepperweed in late summer.

Almost all of the PLSR models predicting instantaneous and daily- and weekly-integrated NEE and GPP had a peak in the VIP score at red wavelengths (Figure 5). Reflectance features within this portion of the spectrum include absorption in the red wavelengths at 642 and 662 nm correlated with chlorophyll absorption, and reflectance in the chlorophyll a fluorescence wavelengths that occurs near 673 nm. The maximum VIP score in the visible wavelengths across nearly all of the PLSR models occurred near the end of the red portion of the spectrum between

670-680 nm, indicating that these wavelengths provided critical information to the latent variables that comprised most of the PLSR models (Figure 5). This result paralleled previous work that demonstrated the importance of narrow-band reflectance at 670-680 nm for predicting chlorophyll absorption features across a diverse suite of plant canopies (Carter and Miller, 1994; Dawson et al., 1999; Gitelson and Merzlyak, 1997; Main et al., 2011).

The differences among the predictive power of the PLSR models that included all the data compared with the models developed at individual sites highlighted important considerations for future work in this area. The predictive models with the smallest 95% prediction intervals originated from the models that included all of the data from both sites (Table 2), demonstrating the power of using larger datasets, with a wider range of values, to develop the predictive capacity of PLSR models. Further improvements in PLSR predictive power might be achieved by building upon this data to include paired hyperspectral-eddy flux datasets from additional sites that can expand and refine the connection between reflectance and CO_2 flux. This approach has particular promise for sites with automated hyperspectral sensing systems in conjunction with eddy covariance measurements (Balzarolo et al., 2011; Hilker et al., 2007; Leuning et al., 2006; Rossini et al., 2010). However, we do emphasize that changes in the canopy complexity and clumping are important consideration for such work at other sites, compared with the short-statured canopies with low clumping indices (Ryu et al., 2010b) included in this study. In canopies with more complex leaf and branch clumping, hyperspectral canopy reflectance measurements will need to be combined with radiative transfer modeling in order to accurately model the energy reflectance spectrum (Knyazikhin et al., 2013; Verhoef and Bach, 2007).

In testing the ability of common SVIs used in the literature to predict GPP and NEE, the skill of some NDVI models were on par with that of the PLSR models when developed using all the data from both sites or the Rice data only (Table 3). We believe that SVIs well-predicted GPP and NEE at the Rice due to its simple annual phenology and corresponding seasonal pattern in CO_2 flux. However, PLSR modeling significantly outperformed SVI models for predicting GPP and NEE flux when developed using only the Pasture data, due to the increased canopy complexity at the Pasture site. At the Pasture, the PLSR approach captured more variance within the dataset through its ability to model more complex relationships across the entire spectrum compared with SVIs, which focus only on two spectral areas. This highlights the improved utility for PLSR modeling compared with the use of SVIs to predict ecosystem CO_2 fluxes from canopies with complex phenological shifts.

4.3 CO_2 flux prediction at various timescales

Across all sets of PLSR models, there was an interesting shift in VIP scores from the visible wavelengths to the NIR wavelengths as the timescale of NEE and GPP integration increased (Figure 5). An increase in structural complexity drives higher NIR reflectivity (Main et al., 2011), and the VIP scores across the suite of PLSR models showed that this structural components of the canopy driving NIR reflectance became increasingly important to predicting both NEE and GPP as the integrated timescale increased. This demonstrated that reflectance in visible wavelengths correlated with chlorophyll content was most important for short-term flux prediction, but canopy structural changes in the NIR wavelengths was most important for longer-term flux prediction. These results are analogous with those from a modeling study across a network of European grassland sites that found a strong correlation between GPP and NIR reflectance indicative of phenological shifts in structural canopy components independent of changes in chlorophyll reflectance (Balzarolo et al., 2015). An important constraint of our analysis is that the field spectrometer used only measured wavelengths up to 900 nm reliably, making analysis at longer wavelengths in the infrared area correlated with leaf structural components such as fiber, lignin, and cellulose content impossible (Serbin et al., 2014). However, this same approach of canopy-level PLSR modeling could be used in conjunction with a spectrometer capable of making wider spectral reflectance measurements at eddy covariance sites to evaluate longer wavelength areas of the short-wave IR (SWIR) spectrum, for example with the newly developed WhiteRef automated sensor for quasi-continuous SWIR hyperspectral measurements (Sakowska et al., 2015).

Comparing the predictive fit achieved with the PLSR models across different CO_2 flux timescales with the Independent Validation dataset provided important insights into the temporal scale of CO_2 flux integration represented by the hyperspectral canopy reflectance collection at a moment in time. Almost all of the final PLSR models achieved the highest predictive fit with the weekly-integrated GPP fluxes (Figure 7). The changes in the PLSR predictive power for NEE and GPP at different timescales provided important information for considering what exactly is represented by measured hyperspectral reflectance in the field, as canopy biochemistry is in fact an emergent response to biological and environmental drivers that are integrated through time. The fact that all three models achieved the best predictive fit with the Independent Validation data for GPP at the weekly timescale yielded support for modeling efforts that determine carbon fluxes from MODIS satellite reflectance, which is aggregated into an 8-day timescale. The results of this flux timescale analysis are congruous with those from previous work, which found a good correlation between gross CO_2 flux and the 8-day MODIS data timescale (Sims et al., 2005). While there was a clear signal in the higher predictive power for estimating the weekly-integrated GPP flux compared with other timescales, there was less consistency within the best predictive timescale for estimating NEE (Figure 7). This is likely due to the fact that NEE is a combination of both GPP and ER, which change on different timescales in response to different environmental drivers and are more highly coupled at the Rice than they are at the Pasture (Hatala et al., 2012; Knox et al., 2014). The fact that NEE achieved a good fit with canopy hyperspectral reflectance through the monthly timescale for the models developed with all the data (Figure 7a) could indicate that the system memory in carbon flux at these sites is integrated over a longer timescale than was tested in this analysis, and that canopy biochemistry collected at one moment reflects at least the previous month of integrated NEE flux.

5. Conclusions

This analysis demonstrated that using PLSR modeling with repeated near-surface hyperspectral canopy reflectance created reliable predictive models of NEE and GPP flux for two short-structured plant canopies with different phenology and significant intra-site and inter-annual variability in canopy reflectance. The PLSR models developed from hyperspectral canopy reflectance collected during 100 site visits from 2010-2014 at a Pasture and a Rice paddy achieved a high level of predictability for both NEE and GPP flux where the predictive R^2 ranged from 0.24 to 0.69 using an independent validation dataset. The higher variability in measured hyperspectral reflectance at the Pasture did decrease the predictive power of the PLSR models when compared against those developed at the Rice site with a more homogeneous canopy. The PLSR models were most skilled at predicting the GPP flux for the integrated week prior to the collection of canopy reflectance. Although the use of PLSR methods with hyperspectral field reflectance such as those presented within this analysis need to be rigorously tested with a much larger dataset and in more diverse ecosystems, the results from this analysis showed promise for using repeated hyperspectral canopy reflectance to directly predict landscape-scale carbon flux. Use of this method, particularly if developed with large datasets collected over several years, might help to constrain GPP estimates through the integration of additional datasets into the modeling efforts that partition NEE into GPP and ER at flux sites (Hilker et al., 2014). The development of PLSR models to predict NEE and GPP from hyperspectral canopy reflectance collected within flux tower footprints is a promising avenue of future research, particularly with the development and deployment of hyperspectral satellite sensors such as NASA's Hyperspectral and InfraRed Imager (HyspIRI; http:// http://hyspiri.jpl.nasa.gov), which will provide continuous spatial coverage of measured hyperspectral reflectance.

6. Author Contributions

D.D.B., J.H.M., and O.S. designed the experiment, all co-authors collected, processed, and analyzed the reflectance and eddy covariance measurements, J.H.M. designed and conducted PLSR modeling, and J.H.M. wrote the manuscript with input from all co-authors.

7. Acknowledgements

The authors would like to thank Bryan Brock and the California Department of Water Resources for funding through DWR contract 4600008849. This research was also supported by the United States Department of Agriculture NIFA grant number 2011-67003-30371, and the National Science Foundation Atmospheric and Geospace Science Program grant AGS-0628720. J.H.M.

thanks the National Science Foundation Graduate Research Fellowship program for support through grant DGE-1106400.

8. Bibliography

Asner, G. and Martin, R.: Spectral and chemical analysis of tropical forests: Scaling from leaf to canopy levels, Remote Sens. Environ., 112(10), 3958–3970, doi:10.1016/j.rse.2008.07.003, 2008a.

Asner, G. P. and Martin, R. E.: Airborne spectranomics: mapping canopy chemical and taxonomic diversity in tropical forests, Front. Ecol. Environ., 7(5), 269–276, doi:10.1890/070152, 2008b.

Baldocchi, D. D., Falge, E., Gu, L. H., Olson, R., Hollinger, D., Running, S., Anthoni, P., Bernhofer, C., Davis, K., Evans, R., Fuentes, J., Goldstein, A., Katul, G., Law, B., Lee, X. H., Malhi, Y., Meyers, T., Munger, W., Oechel, W., U, K. T. P., Pilegaard, K., Schmid, H. P., Valentini, R., Verma, S., Vesala, T., Wilson, K. and Wofsy, S.: FLUXNET: A new tool to study the temporal and spatial variability of ecosystem-scale carbon dioxide, water vapor, and energy flux densities, Bull. Am. Meteorol. Soc., 82(11), 2415–2434 [online] Available from: <Go to ISI>://000171929700004, 2001a.

Baldocchi, D., Falge, E. and Wilson, K.: A spectral analysis of biosphere-atmosphere trace gas flux densities and meteorological variables across hour to multi-year time scales, Agric. For. Meteorol., 107(1), 1–27, doi:10.1016/s0168-1923(00)00228-8, 2001b.

Balzarolo, M., Anderson, K., Nichol, C., Rossini, M., Vescovo, L., Arriga, N., Wohlfahrt, G., Calvet, J.-C., Carrara, A., Cerasoli, S., Cogliati, S., Daumard, F., Eklundh, L., Elbers, J. A., Evrendilek, F., Handcock, R. N., Kaduk, J., Klumpp, K., Longdoz, B., Matteucci, G., Meroni, M., Montagnani, L., Ourcival, J.-M., Sánchez-Cañete, E. P., Pontailler, J.-Y., Juszczak, R., Scholes, B. and Martín, M. P.: Ground-Based Optical Measurements at European Flux Sites: A Review of Methods, Instruments and Current Controversies, Sensors, 11(12), 7954–7981, doi:10.3390/s110807954, 2011.

Balzarolo, M., Vescovo, L., Hammerle, A., Gianelle, D., Papale, D., Tomelleri, E. and Wohlfahrt, G.: On the relationship between ecosystem-scale hyperspectral reflectance and CO_{2} exchange in European mountain grasslands, Biogeosciences, 12(10), 3089–3108, doi:10.5194/bg-12-3089-2015, 2015.

Bauer, M. E.: The role of remote sensing in determining the distribution and yield of crops, Adv. Agron., 27, 271–304, doi:10.1016/s0065-2113(08)70012-9, 1975.

Beget, M. E. and Di Bella, C. M.: Flooding: The effect of water depth on the spectral response of grass canopies, J. Hydrol., 335(3-4), 285–294, doi:10.1016/j.jhydrol.2006.11.018, 2007.

Bolster, K. L., Martin, M. E. and Aber, J. D.: Determination of carbon fraction and nitrogen concentration in tree foliage by near infrared reflectances: a comparison of statistical methods, Can. J. For. Res., 26(4), 590–600, doi:10.1139/x26-068, 1996.

Carter, G. A. and Miller, R. L.: Early detection of plant stress by digital imaging within narrow stress-sensitive wavebands, Remote Sens. Environ., 50(3), 295–302, doi:10.1016/0034-4257(94)90079-5, 1994.

Chen, S., Hong, X., Harris, C. J. and Sharkey, P. M.: Spare modeling using orthogonal forest regression with PRESS statistic and regularization, IEEE Trans. Syst. Man Cybern., 34, 898–911, 2004.

Colwell, J. E.: Vegetation canopy reflectance, Remote Sens. Environ., 3(3), 175–183, doi:10.1016/0034-4257(74)90003-0, 1974.

Dawson, T. P., Curran, P. J., North, P. R. J. and Plummer, S. E.: The Propagation of Foliar Biochemical Absorption Features in Forest Canopy Reflectance, Remote Sens. Environ., 67(2), 147–159, doi:10.1016/S0034-4257(98)00081-9, 1999.

Detto, M., Baldocchi, D. and Katul, G. G.: Scaling Properties of Biologically Active Scalar Concentration Fluctuations in the Atmospheric Surface Layer over a Managed Peatland, Boundary-Layer Meteorol., 136(3), 407–430, doi:10.1007/s10546-010-9514-z, 2010.

Gamon, J. A., Coburn, C., Flanagan, L. B., Huemmrich, K. F., Kiddle, C., Sanchez-Azofeifa, G. A., Thayer, D. R., Vescovo, L., Gianelle, D., Sims, D. A., Rahman, A. F. and Pastorello, G. Z.: SpecNet revisited: bridging flux and remote sensing communities, Can. J. Remote Sens., 36(S2), S376–S390, doi:10.5589/m10-067, 2010.

Gamon, J. A., Penuelas, J. and Field, C. B.: A narrow-waveband spectral index that tracks diurnal changes in photosynthetic efficiency , Remote Sens. Environ., 41(1), 35–44, doi:10.1016/0034-4257(92)90059-s, 1992.

Gamon, J. A., Serrano, L. and Surfus, J. S.: The Photochemical Reflectance Index: An Optical Indicator of Photosynthetic Radiation Use Efficiency across Species, Functional Types, and Nutrient Levels, Oecologia, 112(4), 492–501, doi:10.2307/4221805, 1997.

Gitelson, A. A., Kaufman, Y. J. and Merzlyak, M. N.: Use of a green channel in remote sensing of global vegetation from EOS-MODIS, Remote Sens. Environ., 58(3), 289–298, doi:http://dx.doi.org/10.1016/S0034-4257(96)00072-7, 1996.

Gitelson, A. A. and Merzlyak, M. N.: Remote estimation of chlorophyll content in higher plant leaves, Int. J. Remote Sens., 18(12), 2691–2697, doi:10.1080/014311697217558, 1997.

Gitelson, A. and Merzlyak, M. N.: Spectral Reflectance Changes Associated with Autumn Senescence of Aesculus hippocastanum L. and Acer platanoides L. Leaves. Spectral Features and Relation to Chlorophyll Estimation, J. Plant Physiol., 143(3), 286–292, doi:http://dx.doi.org/10.1016/S0176-1617(11)81633-0, 1994.

Hansen, P. M. and Schjoerring, J. K.: Reflectance measurement of canopy biomass and nitrogen status in wheat crops using normalized difference vegetation indices and partial least squares regression, Remote Sens. Environ., 86(4), 542–553, doi:http://dx.doi.org/10.1016/S0034-4257(03)00131-7, 2003.

Hatala, J. A., Detto, M., Sonnentag, O., Deverel, S. J., Verfaillie, J. and Baldocchi, D.: Greenhouse gas (CO2, CH4, H2O) fluxes from drained and flooded agricultural peatlands in the Sacramento-San Joaquin Delta, Agric. Ecosyst. Environ., 150, 1–18, 2012.

Hestir, E. L., Khanna, S., Andrew, M. E., Santos, M. J., Viers, J. H., Greenberg, J. A., Rajapakse, S. S. and Ustin, S. L.: Identification of invasive vegetation using hyperspectral remote sensing in the California Delta ecosystem, Remote Sens. Environ., 112(11), 4034–4047, doi:10.1016/j.rse.2008.01.022, 2008.

Hilker, T., Coops, N. C., Nesic, Z., Wulder, M. A. and Black, A. T.: Instrumentation and approach for unattended year round tower based measurements of spectral reflectance, Comput. Electron. Agric., 56(1), 72–84, doi:10.1016/j.compag.2007.01.003, 2007.

Hilker, T., Hall, F. G., Coops, N. C., Black, A. T., Jassal, R., Mathys, A. and Grant, N.: Potentials and limitations for estimating daytime ecosystem respiration by combining tower-based remote sensing and carbon flux measurements, Remote Sens. Environ., 150, 44–52, doi:10.1016/j.rse.2014.04.018, 2014.

Inoue, Y., Peñuelas, J., Miyata, A. and Mano, M.: Normalized difference spectral indices for estimating photosynthetic efficiency and capacity at a canopy scale derived from hyperspectral and CO2 flux measurements in rice, Remote Sens. Environ., 112(1), 156–172, doi:10.1016/j.rse.2007.04.011, 2008.

Justice, C. O., Townshend, J. R. G., Holben, B. N. and Tucker, C. J.: Analysis of the phenology of global vegetation using meteorological satellite data, Int. J. Remote Sens., 6(8), 1271–1318, doi:10.1080/01431168508948281, 1985.

Kawamura, K., Watanabe, N., Sakanoue, S. and Inoue, Y.: Estimating forage biomass and quality in a mixed sown pasture based on partial least squares regression with waveband selection, Grassl. Sci., 54(3), 131–145, doi:10.1111/j.1744-697X.2008.00116.x, 2008.

Knox, S. H., Sturtevant, C., Matthes, J. H., Koteen, L., Verfaillie, J. and Baldocchi, D.: Agricultural peatland restoration: effects of land-use change on greenhouse gas (CO2 and CH4) fluxes in the Sacramento-San Joaquin Delta, Glob. Chang. Biol., online ear, doi:10.1111/gcb.12745, 2014.

Knyazikhin, Y., Schull, M. A., Stenberg, P., Mõttus, M., Rautiainen, M., Yang, Y., Marshak, A., Latorre Carmona, P., Kaufmann, R. K., Lewis, P., Disney, M. I., Vanderbilt, V., Davis, A. B., Baret, F., Jacquemoud, S., Lyapustin, A. and Myneni, R. B.: Hyperspectral remote sensing of foliar nitrogen content, Proc. Natl. Acad. Sci., 110(3), E185–E192, doi:10.1073/pnas.1210196109, 2013.

Leuning, R., Hughes, D., Daniel, P., Coops, N. and Newnham, G.: A multi-angle spectrometer for automatic measurement of plant canopy reflectance spectra, Remote Sens. Environ., 103(3), 236–245, doi:10.1016/j.rse.2005.06.016, 2006.

Liu, H. Q. and Huete, A.: A feedback based modification of the NDVI to minimize canopy background and atmospheric noise, Ieee Trans. Geosci. Remote Sens., 33(3), 814 [online] Available from: <Go to ISI>://WOS:A1995RB11400033, 1995.

Lloyd, J. and Taylor, J. A.: On the temperature-dependence of soil respiration, Funct. Ecol., 8(3), 315–323, doi:10.2307/2389824, 1994.

Main, R., Cho, M. A., Mathieu, R., O'Kennedy, M. M., Ramoelo, A. and Koch, S.: An investigation into robust spectral indices for leaf chlorophyll estimation, Isprs J. Photogramm. Remote Sens., 66(6), 751–761, doi:10.1016/j.isprsjprs.2011.08.001, 2011.

Meroni, M., Barducci, A., Cogliati, S., Castagnoli, F., Rossini, M., Busetto, L., Migliavacca, M., Cremonese, E., Galvagno, M., Colombo, R. and Morra di Cella, U.: The hyperspectral irradiometer, a new instrument for long-term and unattended field spectroscopy measurements, Rev. Sci. Instrum., 82, 043106, 2011.

Mevik, B.-H., Wehrens, R. and Liland, K. H.: pls, [online] Available from: http://cran.r-project.org/web/packages/pls/pls.pdf, 2013.

Moffat, A. M., Papale, D., Reichstein, M., Hollinger, D. Y., Richardson, A. D., Barr, A. G., Beckstein, C., Braswell, B. H., Churkina, G., Desai, A. R., Falge, E., Gove, J. H., Heimann, M., Hui, D. F., Jarvis, A. J., Kattge, J., Noormets, A. and Stauch, V. J.: Comprehensive comparison of gap-filling techniques for eddy covariance net carbon fluxes, Agric. For. Meteorol., 147(3-4), 209–232, doi:10.1016/j.agrformet.2007.08.011, 2007.

Moncrieff, J. B., Malhi, Y. and Leuning, R.: Biosphere-atmosphere exchange of CO2 in relation to climate: a cross-biome analysis across multiple time scales, Glob. Chang. Biol., 2(3), 231–240, doi:10.1111/j.1365-2486.1996.tb00075.x, 1996.

Nicodemus, F. E., Richmond, J. C., Hsia, J. J., Ginsberg, I. W. and Limeris, T.: Geometrical Considerations and Nomenclature for Reflectance, Washington, DC., 1977.

Ollinger, S. V, Smith, M. L., Martin, M. E., Hallett, R. A., Goodale, C. L. and Aber, J. D.: Regional variation in foliar chemistry and N cycling among forests of diverse history and composition, Ecology, 83(2), 339–355, doi:10.1890/0012-9658(2002)083[0339:RVIFCA]2.0.CO;2, 2002.

Papale, D., Reichstein, M., Aubinet, M., Canfora, E., Bernhofer, C., Kutsch, W., Longdoz, B., Rambal, S., Valentini, R., Vesala, T. and Yakir, D.: Towards a standardized processing of Net Ecosystem Exchange measured with eddy covariance technique: algorithms and uncertainty estimation, Biogeosciences, 3(4), 571–583 [online] Available from: <Go to ISI>://WOS:000243785300013, 2006.

Potter, C. S., Randerson, J. T., Field, C. B., Matson, P. A., Vitousek, P. M., Mooney, H. A. and Klooster, S. A.: Terrestrial ecosystem production: A process model based on global satellite and surface data, Global Biogeochem. Cycles, 7(4), 811–841, doi:10.1029/93GB02725, 1993.

Reichstein, M., Falge, E., Baldocchi, D., Papale, D., Aubinet, M., Berbigier, P., Bernhofer, C., Buchmann, N., Gilmanov, T., Granier, A., Grunwald, T., Havrankova, K., Ilvesniemi, H., Janous, D., Knohl, A., Laurila, T., Lohila, A., Loustau, D., Matteucci, G., Meyers, T., Miglietta, F., Ourcival, J. M., Pumpanen, J., Rambal, S., Rotenberg, E., Sanz, M., Tenhunen, J., Seufert, G., Vaccari, F., Vesala, T., Yakir, D. and Valentini, R.: On the separation of net ecosystem exchange into assimilation and ecosystem respiration: review and improved algorithm, Glob. Chang. Biol., 11(9), 1424–1439, doi:10.1111/j.1365-2486.2005.001002.x, 2005.

Reichstein, M., Papale, D., Valentini, R., Aubinet, M., Bernhofer, C., Knohl, A., Laurila, T., Lindroth, A., Moors, E., Pilegaard, K. and Seufert, G.: Determinants of terrestrial ecosystem carbon balance inferred from European eddy covariance flux sites, Geophys. Res. Lett., 34(1), n/a–n/a, doi:10.1029/2006GL027880, 2007.

Rossini, M., Meroni, M., Migliavacca, M., Manca, G., Cogliati, S., Busetto, L., Picchi, V., Cescatti, A., Seufert, G. and Colombo, R.: High resolution field spectroscopy measurements for estimating gross ecosystem production in a rice field, Agric. For. Meteorol., 150(9), 1283–1296, doi:10.1016/j.agrformet.2010.05.011, 2010.

Rouse, J. W., Haas, R. H., Schell, J. A. and Deering, D. W.: Monitoring vegetation systems in the Great Plains with ERTS, in 3rd ERTS Symposium, pp. 309–317, NASA SP-351 I., 1974.

Running, S. W., Baldocchi, D. D., Turner, D. P., Gower, S. T., Bakwin, P. S. and Hibbard, K. A.: A global terrestrial monitoring network integrating tower fluxes, flask sampling, ecosystem modeling and EOS satellite data, Remote Sens. Environ., 70(1), 108–127, doi:10.1016/s0034-4257(99)00061-9, 1999.

Running, S. W. and Nemani, R. R.: Relating seasonal patterns of the AVHRR vegetation index to simulated photosynthesis and transpiration of forests in different climates, Remote Sens. Environ., 24(2), 347–367, 1988.

Ryu, Y., Baldocchi, D. D., Verfaillie, J., Ma, S., Falk, M., Ruiz-Mercado, I., Hehn, T. and Sonnentag, O.: Testing the performance of a novel spectral reflectance sensor, built with light emitting diodes (LEDs), to monitor ecosystem metabolism, structure and function, Agric. For. Meteorol., 150(12), 1597–1606, doi:http://dx.doi.org/10.1016/j.agrformet.2010.08.009, 2010a.

Ryu, Y., Nilson, T., Kobayashi, H., Sonnentag, O., Law, B. E. and Baldocchi, D. D.: On the correct estimation of effective leaf area index: Does it reveal information on clumping effects?, Agric. For. Meteorol., 150(3), 463–472, doi:10.1016/j.agrformet.2010.01.009, 2010b.

Sakowska, K., Gianelle, D., Zaldei, A., MacArthur, A., Carotenuto, F., Miglietta, F., Zampedri, R., Cavagna, M. and Vescovo, L.: WhiteRef: A new tower-based hyperspectral system for continuous reflectance measurements, Sensors, 15, 1088–1105, doi:10.3390/s150101088, 2015.

Schaepman-Strub, G., Schaepman, M. E., Painter, T. H., Dangel, S. and Martonchik, J. V.: Reflectance quantities in optical remote sensing—definitions and case studies, Remote Sens. Environ., 103(1), 27–42, doi:10.1016/j.rse.2006.03.002, 2006.

Schmidtlein, S., Zimmermann, P., Schüpferling, R. and Weiß, C.: Mapping the floristic continuum: Ordination space position estimated from imaging spectroscopy, J. Veg. Sci., 18(1), 131–140, doi:10.1111/j.1654-1103.2007.tb02523.x, 2007.

Schotanus, P., Nieuwstadt, F. T. M. and Debruin, H. A. R.: Temperature measurement with a sonic anemometer and its application to heat and moisture fluxes, Boundary-Layer Meteorol., 26(1), 81–93 [online] Available from: <Go to ISI>://WOS:A1983QX37400006, 1983.

Serbin, S. P., Dillaway, D. N., Kruger, E. L. and Townsend, P. A.: Leaf optical properties reflect variation in photosynthetic metabolism and its sensitivity to temperature, J. Exp. Bot., 63(1), 489–502, doi:10.1093/jxb/err294, 2012.

Serbin, S. P., Singh, A., McNeil, B. E., Kingdon, C. C. and Townsend, P. A.: Spectroscopic determination of leaf morphological and biochemical traits for northern temperate and boreal tree species, Ecol. Appl., doi:10.1890/13-2110.1, 2014.

Sims, D. A., Rahman, A. F., Cordova, V. D., Baldocchi, D. D., Flanagan, L. B., Goldstein, A. H., Hollinger, D. Y., Misson, L., Monson, R. K., Schmid, H. P., Wofsy, S. C. and Xu, L.: Midday values of gross CO2 flux and light use efficiency during satellite overpasses can be used to directly estimate eight-day mean flux, Agric. For. Meteorol., 131(1-2), 1–12, doi:10.1016/j.agrformet.2005.04.006, 2005.

Smith, M.-L., Ollinger, S. V, Martin, M. E., Aber, J. D., Hallett, R. A. and Goodale, C. L.: Direct estimation of aboveground forest productivity through hyperspectral remote sensing of canopy nitrogen, Ecol. Appl., 12(5), 1286–1302, doi:10.1890/1051-0761(2002)012[1286:DEOAFP]2.0.CO;2, 2002.

Sonnentag, O., Detto, M., Runkle, B. R. K., Teh, Y. A., Silver, W. L., Kelly, M. and Baldocchi, D. D.: Carbon dioxide exchange of a pepperweed (Lepidium latifoliumL.) infestation: How do flowering and mowing affect canopy photosynthesis and autotrophic respiration?, J. Geophys. Res., 116(G1), doi:10.1029/2010jg001522, 2011a.

Sonnentag, O., Detto, M., Vargas, R., Ryu, Y., Runkle, B. R. K., Kelly, M. and Baldocchi, D. D.: Tracking the structural and functional development of a perennial pepperweed (Lepidium latifolium L.) infestation using a multi-year archive of webcam imagery and eddy covariance measurements, Agric. For. Meteorol., 151(7), 916–926, doi:10.1016/j.agrformet.2011.02.011, 2011b.

Stoy, P. C., Richardson, A. D., Baldocchi, D. D., Katul, G. G., Stanovick, J., Mahecha, M. D., Reichstein, M., Detto, M., Law, B. E., Wohlfahrt, G., Arriga, N., Campos, J., McCaughey, J. H., Montagnani, L., Paw U, K. T., Sevanto, S. and Williams, M.: Biosphere-atmosphere exchange of

CO2 in relation to climate: a cross-biome analysis across multiple time scales, Biogeosciences, 6(10), 2297–2312, doi:10.5194/bg-6-2297-2009, 2009.

Tucker, C. J., Townshend, J. R. G. and Goff, T. E.: African land-cover classification using satellite data, Science (80-.)., 227(4685), 369–375, 1985.

Ustin, S. L., Roberts, D. A., Gamon, J. A., Asner, G. P. and Green, R. O.: Using Imaging Spectroscopy to Study Ecosystem Processes and Properties, Bioscience, 54(6), 523–534, doi:10.1641/0006-3568(2004)054[0523:UISTSE]2.0.CO;2, 2004.

Verhoef, W. and Bach, H.: Coupled soil–leaf-canopy and atmosphere radiative transfer modeling to simulate hyperspectral multi-angular surface reflectance and TOA radiance data, Remote Sens. Environ., 109(2), 166–182, doi:10.1016/j.rse.2006.12.013, 2007.

Webb, E. K., Pearman, G. I. and Leuning, R.: Correction of flux measurements for density effects due to heat and water-vapor transfer, Q. J. R. Meteorol. Soc., 106(447), 85–100 [online] Available from: <Go to ISI>://WOS:A1980JD79200007, 1980.

Wold, S., Sjostrom, M. and Eriksson, L.: PLS-regression: a basic tool of chemometrics, Chemom. Intell. Lab. Syst., 58, 109–130, 2001.

Yang, X., Tang, J. and Mustard, J. F.: Beyond leaf color: Comparing camera-based phenological metrics with leaf biochemical, biophysical, and spectral properties throughout the growing season of a temperate deciduous forest, J. Geophys. Res. Biogeosciences, 119(3), 181–191, doi:10.1002/2013JG002460, 2014.

Ye, X., Sakai, K., Sasao, A. and Asada, S.: Estimation of citrus yield from canopy spectral features determined by airborne hyperspectral imagery, Int. J. Remote Sens., 30(18), 4621–4642, doi:10.1080/01431160802632231, 2009.

Table 1. Fit statistics for the bootstrapped PLSR model. The mean R^2 and root mean squared error (RMSE) is provided for the PLSR Calibration fitting (Cal) and the calibration Evaluation (Eval) during the PLSR model development, conducted with 80% of the total dataset. Units for instantaneous fluxes are μmol m^{-2} s^{-1}, and for daily, weekly, and monthly values are g-C m^{-2}. In general, models with daily-integrated GPP and NEE had the best fit compared with models that fit the flux data from other timescales. The PLSR fit for GPP using the hyperspectral reflectance data tended to outperform the fit of NEE across the datasets and models. The statistical fit of the PLSR models was higher at the Rice site compared with the Pasture.

		R^2 Cal	**R^2 Eval**	**RMSE Cal**	**RMSE Eval**	**Components**
Both sites	GPP inst	0.87	0.64	3.34	4.74	7
	GPP daily	0.87	0.69	1.42	1.96	6
	GPP wkly	0.86	0.69	10.35	13.82	6
	GPP mthly	0.63	0.24	45.47	44.75	6
	NEE inst	0.84	0.64	3.30	4.39	6
	NEE daily	0.84	0.66	1.43	1.87	6
	NEE wkly	0.83	0.65	10.34	13.21	6
	NEE mthly	0.81	0.64	42.11	51.88	6
Pasture	GPP inst	0.94	0.49	1.36	3.49	7
	GPP daily	0.97	0.56	0.43	1.53	8
	GPP wkly	0.53	0.38	11.64	10.15	3
	GPP mthly	0.91	0.42	22.96	52.43	7
	NEE inst	0.43	0.33	3.56	2.52	2
	NEE daily	0.38	0.30	1.40	0.91	2
	NEE wkly	0.44	0.29	8.47	6.42	3
	NEE mthly	0.79	0.36	22.81	30.49	6
Rice	GPP inst	0.85	0.61	4.34	5.92	5
	GPP daily	0.92	0.65	1.34	2.58	6
	GPP wkly	0.84	0.67	13.32	17.06	4
	GPP mthly	0.89	0.68	10.96	16.95	5
	NEE inst	0.77	0.58	4.88	5.66	4
	NEE daily	0.86	0.60	1.68	2.52	5
	NEE wkly	0.85	0.59	11.82	17.88	5

	NEE mthly	0.80	0.64	56.50	67.93	4

Table 2. Independent validation dataset fit for mean PLSR models. We calculated the R^2 and bias between the predicted CO_2 flux variables with the mean PLSR models and the actual measurements from the 20% of data left for Independent Validation. Units for instantaneous fluxes are μmol m^{-2} s^{-1}, and for daily, weekly, and monthly values are g-C m^{-2}. The highest predictive fit for the PLSR models was achieved with the dataset that included the Rice data only.

		R^2		**Bias**	
		NEE	GPP	NEE	GPP
Both sites	Inst	0.51	0.42	-1.63	3.89
	Daily	0.52	0.52	-0.41	1.60
	Weekly	0.55	0.62	-3.31	9.75
	Monthly	0.57	0.27	-11.92	31.51
Pasture	Inst	0.53	0.24	-2.28	5.10
	Daily	0.44	0.45	-0.56	2.79
	Weekly	0.51	0.54	-1.96	15.94
	Monthly	0.43	0.47	-14.18	76.86
Rice	Inst	0.51	0.40	-1.41	2.73
	Daily	0.65	0.50	-0.89	0.58
	Weekly	0.69	0.62	-2.35	0.21
	Monthly	0.41	0.45	-18.56	4.60

Table 3. Comparison of SVIs and PLSR model skill. We evaluated the ability of the commonly used standardized vegetation indices (SVIs) to predict GPP and NEE in comparison with the PLSR models. Here we show the calibration fit R^2 (fit) and predictive R^2 (pred) values for the widely used MODIS NDVI ($NDVI_{MOD}$) and the red-edge NDVI ($NDVI_{re}$), which was the SVI that achieved the highest skill at predicting GPP and NEE. Results from all SVIs tested in this study are included as Supplementary Table 1.

Site	Flux	$NDVI_{MOD}$ fit	$NDVI_{re}$ fit	PLSR fit	$NDVI_{MOD}$ pred	$NDVI_{re}$ pred	PLSR pred
All	GPP_inst	0.50	0.57	0.87	0.18	0.22	0.42
All	GPP_day	0.55	0.65	0.87	0.44	0.53	0.52
All	GPP_week	0.56	0.64	0.86	0.42	0.50	0.62
All	GPP_month	0.49	0.56	0.63	0.32	0.38	0.27
All	NEE_inst	0.49	0.57	0.84	0.50	0.57	0.51
All	NEE_day	0.45	0.54	0.84	0.51	0.58	0.52
All	NEE_week	0.48	0.56	0.83	0.53	0.59	0.55
All	NEE_month	0.53	0.58	0.81	0.54	0.59	0.57
Pasture	GPP_inst	0.29	0.38	0.94	0.09	0.13	0.24
Pasture	GPP_day	0.35	0.45	0.97	0.26	0.34	0.45
Pasture	GPP_week	0.29	0.38	0.53	0.22	0.30	0.54
Pasture	GPP_month	0.18	0.25	0.91	0.13	0.19	0.47
Pasture	NEE_inst	0.31	0.40	0.43	0.30	0.39	0.53
Pasture	NEE_day	0.31	0.41	0.38	0.26	0.35	0.44
Pasture	NEE_week	0.29	0.36	0.44	0.25	0.31	0.51
Pasture	NEE_month	0.20	0.25	0.79	0.17	0.22	0.43
Rice	GPP_inst	0.46	0.54	0.85	0.48	0.49	0.4
Rice	GPP_day	0.56	0.69	0.92	0.57	0.62	0.5
Rice	GPP_week	0.60	0.72	0.84	0.62	0.65	0.62
Rice	GPP_month	0.59	0.68	0.89	0.60	0.63	0.45
Rice	NEE_inst	0.47	0.56	0.77	0.49	0.52	0.51
Rice	NEE_day	0.49	0.60	0.86	0.51	0.55	0.65
Rice	NEE_week	0.54	0.64	0.85	0.56	0.58	0.69
Rice	NEE_month	0.60	0.69	0.8	0.63	0.64	0.41

Figure captions

Figure 1. Canopy hyperspectral field collection dates. This analysis synthesized canopy hyperspectral reflectance measurements collected from 2010-2014 at Pasture and Rice sites in the Sacramento-San Joaquin Delta in Northern California. On each sampling date we collected nine individual canopy hyperspectral reflectance replicates at the Pasture site and five individual reflectance replicates at the Rice site.

Figure 2. Instantaneous gross primary productivity (GPP) and daily net CO_2 flux on the hyperspectral canopy reflectance sampling dates. Both the Pasture and the Rice exhibited strong seasonal patterns with peak CO_2 uptake mid-year. However, the Pasture experienced peak CO_2 uptake that preceded the peak for the Rice, where the maximum CO_2 uptake occurred in March-April for the Pasture and in July-August for the Rice.

Figure 3. Daily variability in measured canopy hyperspectral reflectance during phenological events. a-b) Daily measured hyperspectral canopy reflectance for the Pasture and Rice sites when the canopy was closed and green, at the Pasture on 10 April 2014 and the Rice on 31 July 2013. Reflectance was very low in the visible wavelengths due to canopy absoption, but quite large in the near infrared reflectance with a high amount of variability. Both sites had spectral peaks that corresponded to green reflectance (~550 nm) and troughs that corresponded to spectral absorption in red reflectance (~675 nm). **c)** During the white flowering of the pepperweed plants, the measured reflectance changed significantly, due to the higher albedo of the bright white flowers. There was much higher reflectance across the spectrum during this time, and the white flowers obfuscated reflectance in the wavelengths that corresponded to plant

productivity. **d)** There was a similar but not as dramatic shift in increased albedo particularly across the visible wavelengths from green to red reflectance during the rice seeding and senescence as the canopy dried before harvest. However an important distinction between this phenological event and the white flowering at the Pasture is that the productivity of the rice plants was quite low at this time, in contrast with the higher productivity of the pepperweed during flowering.

Figure 4. Inter-annual and daily variability at narrow-band green, red, and near-infrared (NIR) reflectance. a-b) Inter-annual variability in measured canopy green reflectance at 550±5 nm, where the points are the site mean and the bars represent one standard deviation for each sampling date. The green reflectance at the Pasture was relatively uniform throughout the year, due to the presence of either grass or pepperweed canopy for most of the year. There was more intra-site variability in reflectance during the summer when the pepperweed canopy was active, since at some locations the white flowers of the pepperweed plant can complicate the green reflectance spectrum. The green reflectance at the Rice had more inter-annual variability but a more discernible seasonal pattern within each year, where the trough in green reflectance tended to occur mid-summer. **c-d)** These plots show red reflectance at 662±5 nm at each site, which corresponds to the absorption wavelength of chlorophyll b. Both sites demonstrated a seasonal pattern, where the minimum in red reflectance occured in late spring at the Pasture and in late summer at the Rice, corresponding to the times of peak plant growth at each site. Again, the Pasture had more intra-site variability, particularly during the summer months when pepperweed is active. **e-f)** Here we plot the near infrared (NIR) reflectance at 800±5 nm for the two sites. NIR reflectance at the Pasture had no strong seasonal pattern, with a constant mean throughout the

year and across years. The rice demonstrated a stronger pattern across the season, with less NIR reflectance early in the growing season when the canopy was developing, with higher NIR reflectance as the crop achieved a full canopy later in the summer. At both sites, intra-site variability in NIR reflectance was much higher than the variability in the reflectance in the visible spectrum.

Figure 5. Variable importance of projection (VIP) statistics for bootstrapped partial least-squared regression (PLSR) modeling coefficients. Here we show the variable importance of projection (VIP) statistics for the mean bootstrapped PLSR models, fitted to the GPP and NEE flux datasets. The VIP statistic describes the relative contribution of each wavelength to the predictive power of the PLSR model across all final PLSR model components. Across all models, the visible wavelengths (400-700nm) were most important for prediction at shorter timescales of integrated flux, while the infrared wavelengths (700-900nm) became increasingly important at longer integrated flux intervals. This pattern is particularly apparent within the PLSR model for GPP fitted across All the data (Figure 5a), where there was a dramatic shift in the VIP statistics between the weekly- and monthly-integrated flux prediction and the infrared wavelengths become much more important for prediction at longer timescales. This pattern was also apparent with the PLSR models developed using the Pasture data only. The PLSR models developed for the Rice data only (Figures 5e-f) had the least variation for fluxes integrated at different timescales.

Figure 6. Predictive ability of PLSR models on independent validation dataset. The mean PLSR models determined through the bootstrapping routine were tested on the Independent

Validation dataset, which was composed of 20% of the original data that was separated from the model calibration process. Here the independent validation is presented for instantaneous and daily NEE and GPP flux for the exercises with all the data, Pasture only, and Rice only. The regression line between the predicted and actual variables is black, the 1:1 line is dashed, the 95% credible interval of the regression are the curved dotted lines, and the 95% prediction interval are the grey lines.

Figure 7. Predictive power of measured hyperspectral reflectance at increasing CO_2 flux integration intervals. We examined the ability of PLSR modeling with the hyperspectral reflectance data to predict instantaneous and daily-, weekly-, and monthly-integrated NEE and GPP at **a)** both sites will the entire dataset, **b)** the Pasture only, and **c)** the Rice only. For all three cases, the measured hyperspectral reflectance had the highest correlation with weekly-integrated GPP flux. The time interval with the highest predictive power for NEE flux was less variable across different timescales within each modeling exercise, and there was not a strong improvement to using one particular timescale to model NEE with the hyperspectral reflectance data.

FIGURE 1

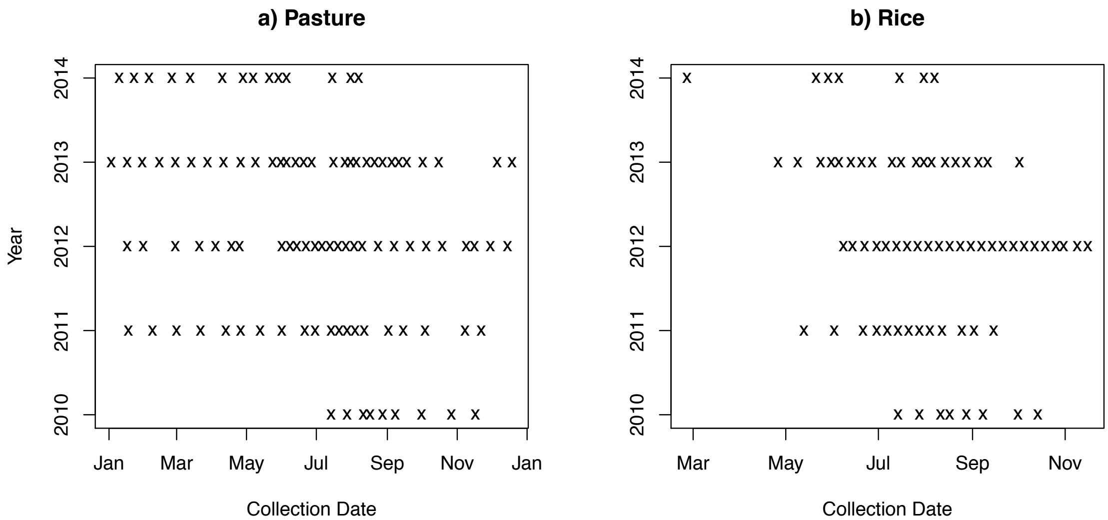
a) Pasture
b) Rice
Year
2010
2011
2012
2013
2014
Jan
Mar
May
Jul
Sep
Nov
Collection Date

FIGURE 2

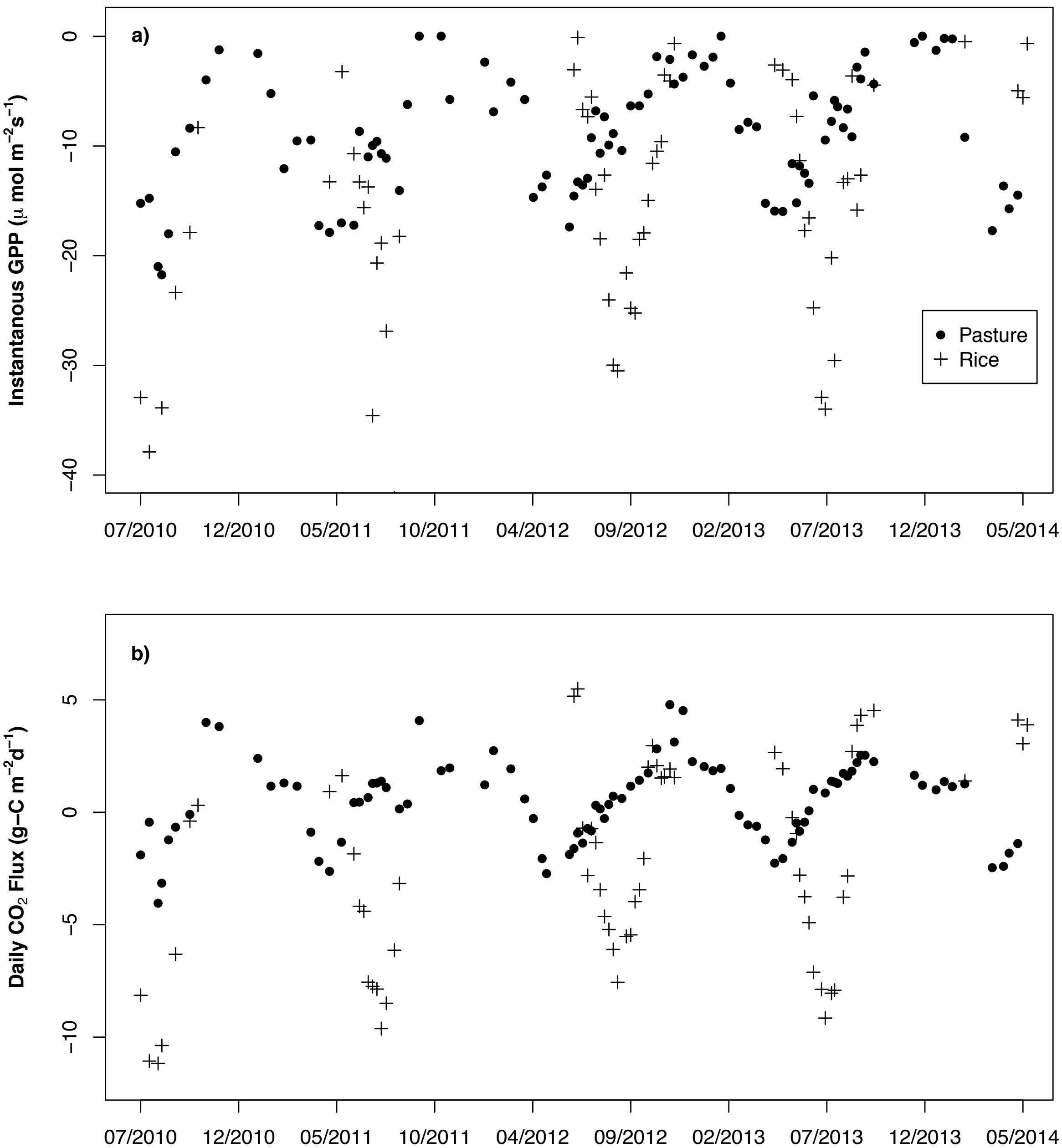
a)
Instantanous GPP (μ mol m^{-2}s^{-1})
0
−10
−20
−30
−40
Pasture
Rice
07/2010
12/2010
05/2011
10/2011
04/2012
09/2012
02/2013
07/2013
12/2013
05/2014
b)
Daily CO_2 Flux (g−C m^{-2}d^{-1})
5
0
−5
−10
07/2010
12/2010
05/2011
10/2011
04/2012
09/2012
02/2013
07/2013
12/2013
05/2014

FIGURE 3

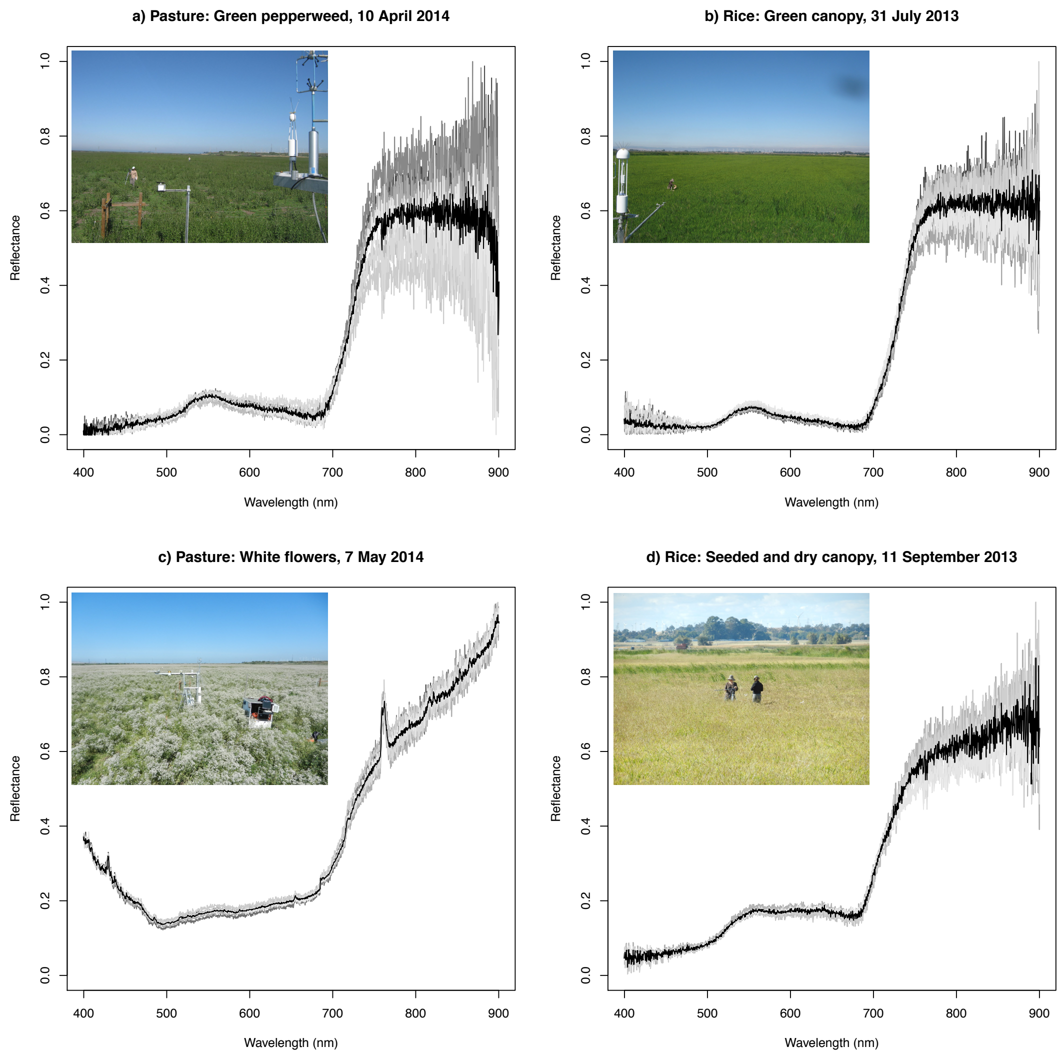

a) Pasture: Green pepperweed, 10 April 2014
b) Rice: Green canopy, 31 July 2013
c) Pasture: White flowers, 7 May 2014
d) Rice: Seeded and dry canopy, 11 September 2013
Reflectance
0.0
0.2
0.4
0.6
0.8
1.0
Wavelength (nm)
400
500
600
700
800
900

FIGURE 4

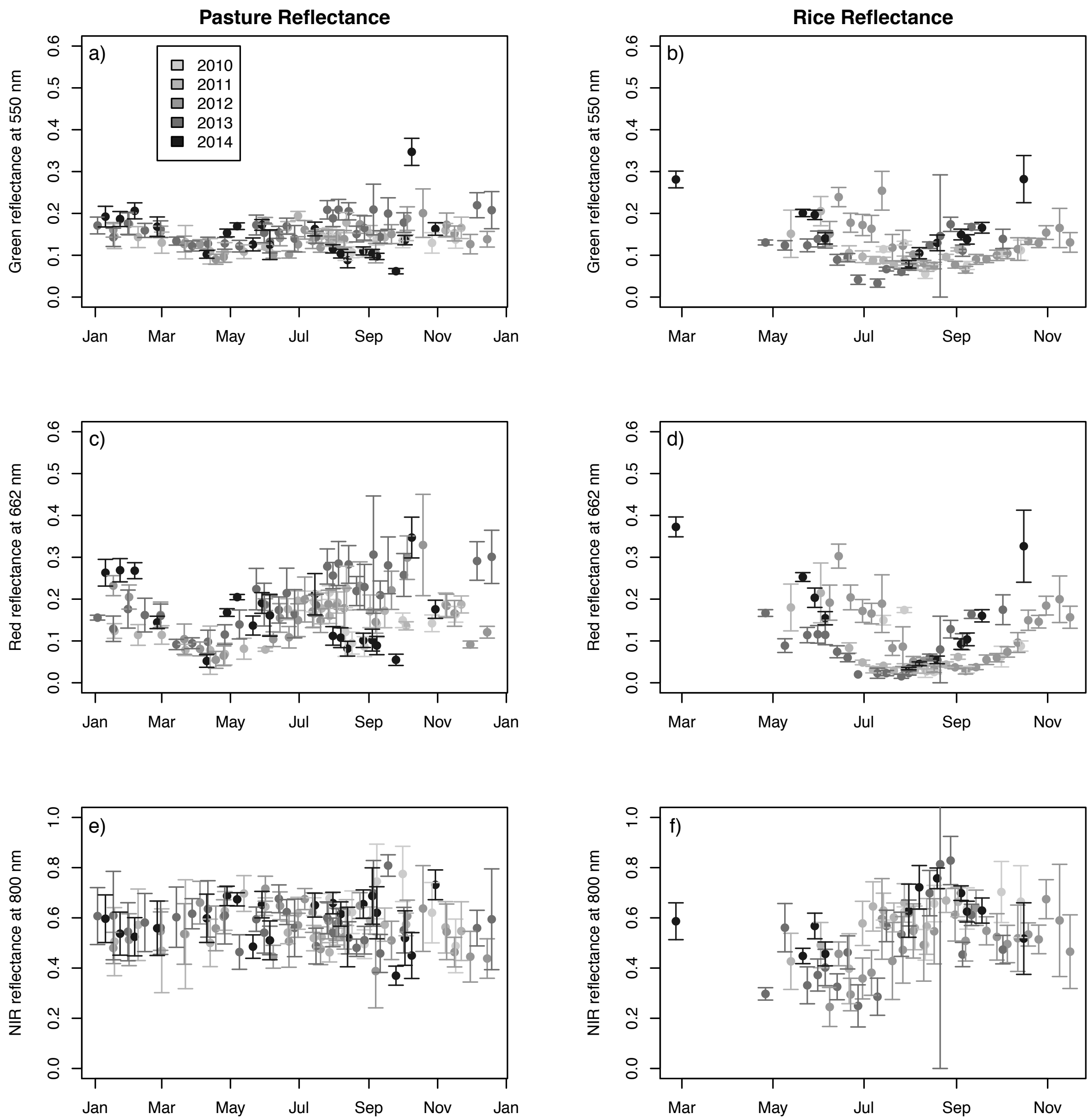
Pasture Reflectance
Rice Reflectance
a)
b)
c)
d)
e)
f)
2010
2011
2012
2013
2014
Green reflectance at 550 nm
Red reflectance at 662 nm
NIR reflectance at 800 nm
0.0 0.1 0.2 0.3 0.4 0.5 0.6
0.0 0.2 0.4 0.6 0.8 1.0
Jan Mar May Jul Sep Nov Jan
Mar May Jul Sep Nov

FIGURE 5

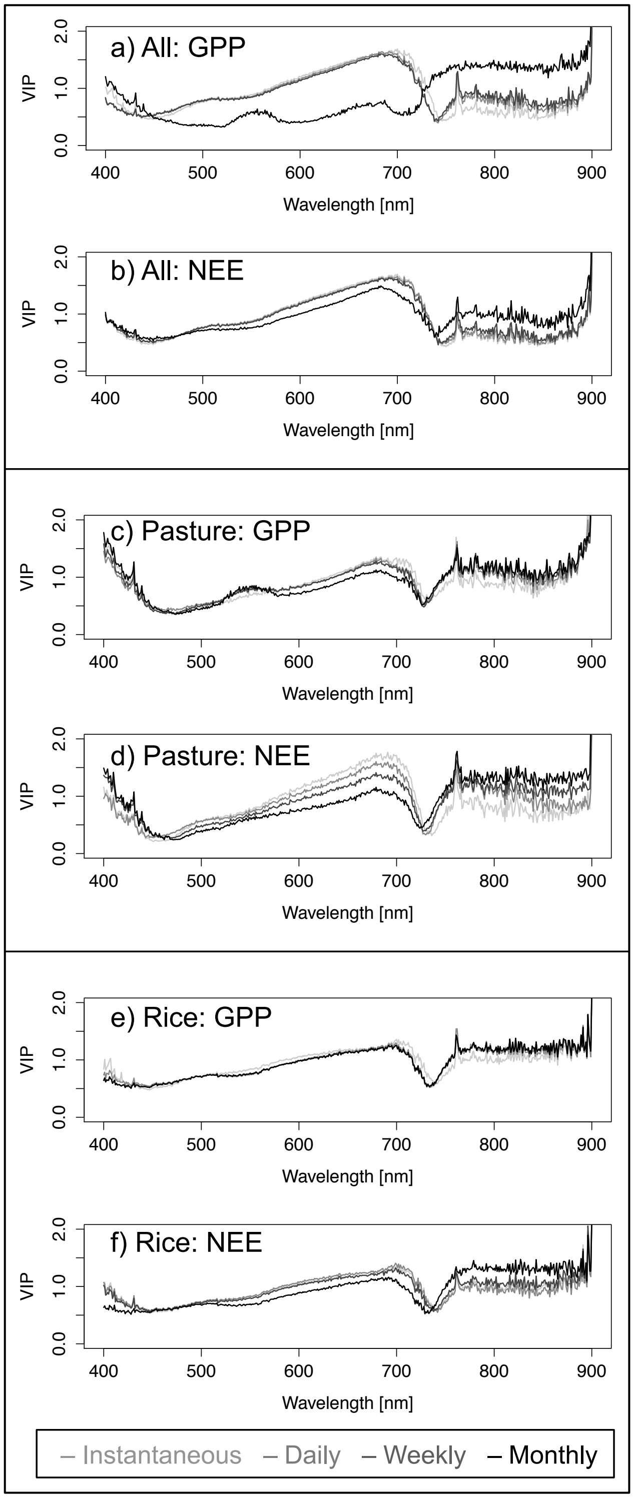
a) All: GPP
b) All: NEE
c) Pasture: GPP
d) Pasture: NEE
e) Rice: GPP
f) Rice: NEE
VIP
0.0
1.0
2.0
400
500
600
700
800
900
Wavelength [nm]
– Instantaneous – Daily – Weekly – Monthly

FIGURE 6

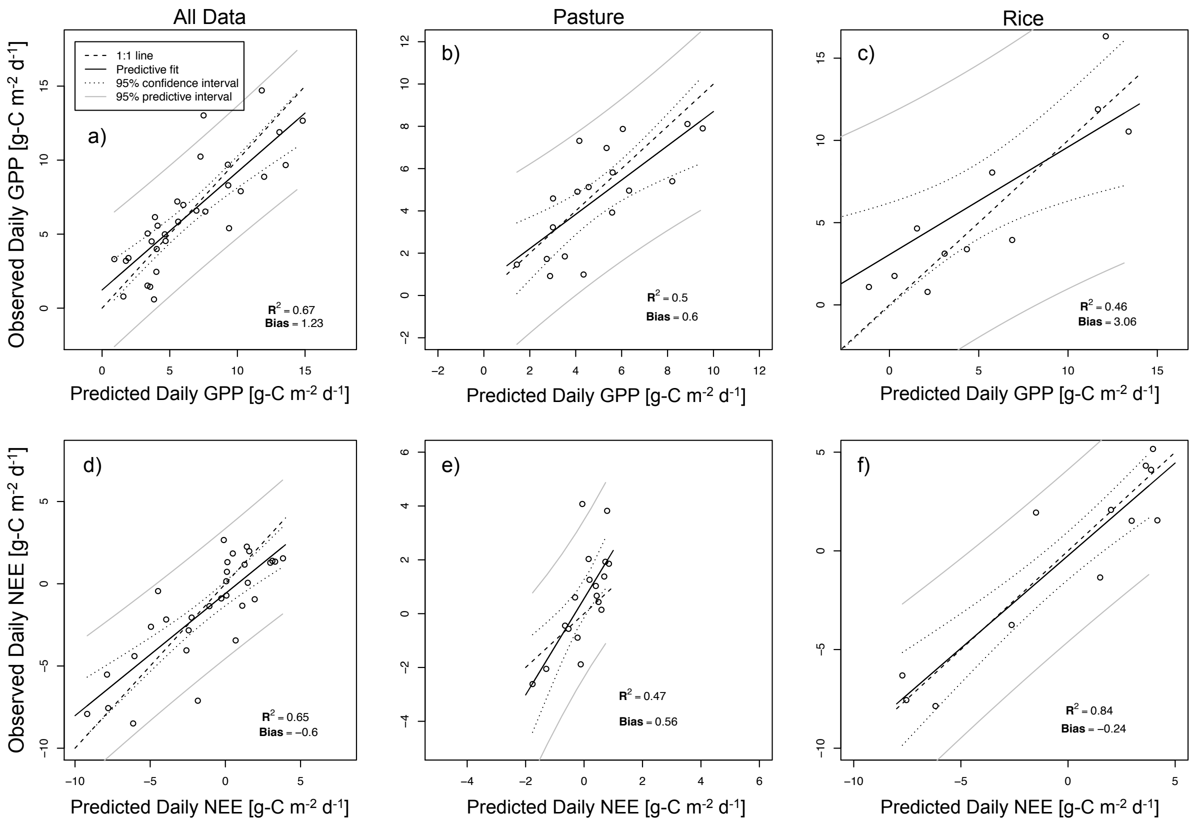
All Data
Pasture
Rice
1:1 line
Predictive fit
95% confidence interval
95% predictive interval
a)
b)
c)
d)
e)
f)
R^2 = 0.67
Bias = 1.23
R^2 = 0.5
Bias = 0.6
R^2 = 0.46
Bias = 3.06
R^2 = 0.65
Bias = −0.6
R^2 = 0.47
Bias = 0.56
R^2 = 0.84
Bias = −0.24
Observed Daily GPP [g-C m^{-2} d^{-1}]
Predicted Daily GPP [g-C m^{-2} d^{-1}]
Observed Daily NEE [g-C m^{-2} d^{-1}]
Predicted Daily NEE [g-C m^{-2} d^{-1}]

FIGURE 7

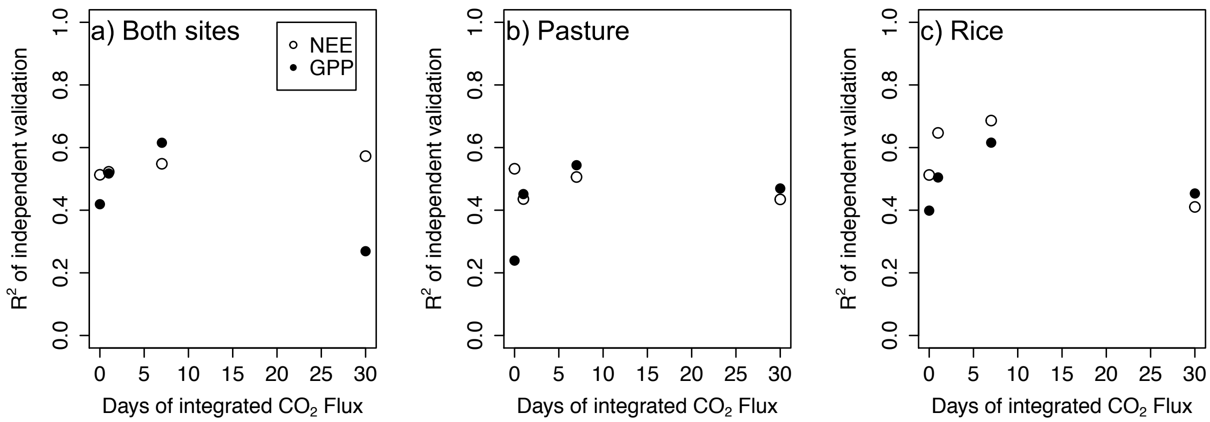

a) Both sites
NEE
GPP
b) Pasture
c) Rice
R^2 of independent validation
Days of integrated CO_2 Flux
0.0
0.2
0.4
0.6
0.8
1.0
0
5
10
15
20
25
30